Central/eastern North Pacific photochemical precursor distributions for fall/spring seasons as defined by airborne field studies

B. DiNunno,[1] D. Davis,[1] G. Chen,[1] G. Gregory,[2] G. Sachse,[2] B. Anderson,[2] S. Vay,[2] M. Avery,[2] B. Ridley,[3] M. Carroll,[4] J. Walega,[3] D. Montzka,[3] F. Grahek,[3] J. Bradshaw,[1,5] S. Sandholm,[1] Y. Kondo,[6] G. Kok,[7] D. Blake,[8] N. Blake,[8] J. Barrick,[2] H. Fuelberg,[9] B. Martin,[9] and A. Balok[2]

Received 9 July 2001; revised 5 April 2002; accepted 10 April 2002; published 30 January 2003.

[1] Data from 10 aircraft programs recorded over the central/eastern North Pacific (180°–120°W, 0°–45°N) were assembled for the purpose of assessing an atmospheric chemical climatology for this region. It represents an early effort at carrying out this task and, thus, it can be expected to undergo many updates in the future. Such a database is useful in both gaining further insights concerning the fundamental processes controlling the chemistry of this region as well as serving as an important baseline by which to evaluate future change. Critical photochemical precursors examined included O_3, CO, NO_x, and H_2O. In addition, the distribution profiles for select nonmethane hydrocarbons were explored. The precursor data were analyzed according to latitude, pressure altitude, and season of the year. Contrasting the spring and fall measurements, major trends that surfaced in both ozone and CO included observing elevated levels in spring compared to fall, with the largest spring increase occurring at latitudes north of 15°N. Both NO_x and H_2O showed trends quite different from that of CO and O_3, with an indication of higher mixing ratio levels during the fall season. Variations in precursor distribution patterns within a season will be explained based on climatological flow patterns for the region and the resulting connection to source regions. Where possible, comparisons were performed with other sampling strategies, including ground-based observations, sonde, and satellite data, and data collected during shuttle missions. Overall, these comparisons revealed a reasonably high level of correspondence between the airborne ensemble data and those collected using other sampling strategies. *INDEX TERMS:* 0368 Atmospheric Composition and Structure: Troposphere—constituent transport and chemistry; 1610 Global Change: Atmosphere (0315, 0325); 9355 Information Related to Geographic Region: Pacific Ocean; *KEYWORDS:* Ozone, Pacific, troposphere, photochemistry

Citation: DiNunno, B., et al., Central/eastern North Pacific photochemical precursor distributions for fall/spring seasons as defined by airborne field studies, *J. Geophys. Res., 108*(D2), 8240, doi:10.1029/2001JD001044, 2003.

1. Introduction

[2] While coming under increasing pressure from anthropogenic influences, the Pacific basin still defines one of the largest pristine areas left in the world, and thus offers the potential for providing an atmospheric chemical baseline by which future change can be measured. It is estimated that in the near future anthropogenic emissions will substantially increase in the North Pacific (the principal area of this study), reflecting estimates showing energy use in eastern Asia as having increased at a rate of 5% per year for the past decade [*Horowitz and Jacob*, 1999]. A continuation in this increase is expected to lead to increases in NO_x, CO, and NMHC's emissions which, in turn, could further modify the atmosphere in terms of the levels of ozone and other oxidants [*Jacob et al.*, 1999; *Jaffe et al.*, 1999].

[3] Tropospheric patterns of ozone have been the focus of research for decades [e.g., *Fishman and Crutzen*, 1978; *Liu et al.*, 1980; *Logan et al.*, 1981; *Levy et al.*, 1985; *Chameides et al.*, 1987; 1989; *Thompson et al.*, 1993; *Davis et al.*, 1996; *Crawford et al.*, 1997b; *Marenco et al.*, 1998; *Schultz et al.*, 1999; *Lelieveld and Dentener*, 2000]. A major issue addressed in much of this earlier work has involved the sorting out of the relative roles of photochemistry and

[1]Department of Earth and Atmospheric Science, Georgia Institute of Technology, Atlanta, Georgia, USA.
[2]NASA Langley Research Center, Hampton, Virginia, USA.
[3]Atmospheric Chemistry Division, National Center for Atmospheric Research, Boulder, Colorado, USA.
[4]Department of Atmospheric, Oceanic, and Space Sciences, University of Michigan, Ann Arbor, Michigan, USA.
[5]Deceased 16 June 1997.
[6]Research Center for Advanced Science and Technology, University of Tokyo, Japan.
[7]Research Aviation Facility, National Center for Atmospheric Research, Boulder, Colorado, USA.
[8]Department of Chemistry, University of California, Irvine, California, USA.
[9]Department of Meteorology, Florida State University, Tallahassee, Florida, USA.

0148-0227/03/2001JD001044$09.00

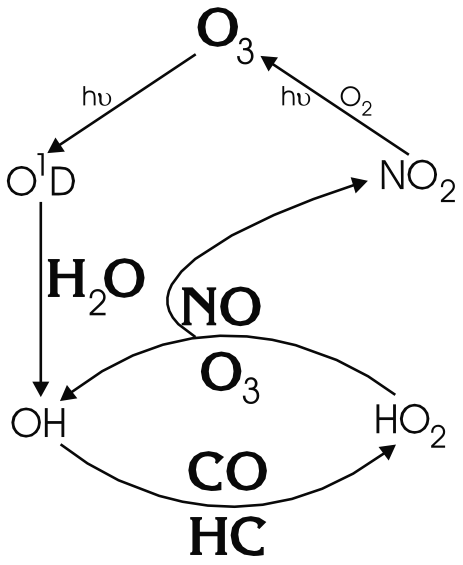

Figure 1. Simplified chemical scheme showing relationship between photochemical precursors and ozone.

stratospheric transport in controlling ozone levels in the troposphere. Of particular interest has been explaining the presence of the late winter-early spring northern hemispheric maximum in midlatitude ozone [*Yienger et al.*, 1999; *Monks*, 2000, and references therein]. More recently the issue of the effect of long range transport of Asian generated ozone precursors on west coast USA ozone levels has also been raised [*Jacob et al.*, 1999; *Jaffe et al.*, 1999; *Yienger et al.*, 1999].

[4] Centrally important to chemically assessing each of these ozone issues is having available reliable northern hemispheric distributions of ozone precursor species. The most critical of these are shown in Figure 1 and, for marine regions, include H_2O, CO, NO_x and O_3. Also indicated as potentially important are NMHC's. However, this chemical family's importance, appears to only become significant as continental land areas are approached. As discussed below, the current effort will be focused only on the northeastern Pacific ocean basin.

[5] Numerous aircraft field campaigns have been conducted in the Pacific basin from which a precursor database can be assembled. One of the earliest of these goes back to project GAMETAG [*Davis*, 1980]. GAMETAG, like many of the programs that followed, passed through the central and eastern North Pacific on their way to specific study regions (see Figure 2). The two Pacific Exploratory Missions West (PEM-West A and B) programs focused on the northwestern Pacific with special emphasis on the Asian Pacific rim [*Hoell et al.*, 1996, 1997]. The first Aerosol Characterization Experiment (ACE 1) examined the Southern Ocean [*Bates et al.*, 1998]. PEM-Tropics A and B [*Hoell et al.*, 1999; *Raper et al.*, 2001] explored the chemistry of the tropical Pacific as did the second Mauna Loa Observatory Photochemistry Experiment (MLOPEX II) which was focused on the island of Hawaii [*Atlas and Ridley*, 1996]. By contrast, the Chemical Instrumentation Test and Evaluation programs (CITE-1C and CITE-2) sampled primarily the eastern North Pacific, with much of this activity occurring just off the coast of California [*Hoell et al.*, 1990]. CITE-1B [*Beck et al.*, 1987] sampled both off the coast of California as well as the region surrounding Hawaii.

[6] The specific area of interest in this study is the central/eastern North Pacific (CENP) as defined by the coordinates 180°–120°W and 0°–45°N. The chemical climatology derived from the past 20 years of aircraft measurements should prove especially useful in establishing baseline values for future research studies, in particular for comparisons to future satellite observations [*Connors et al.*, 1999]. In a companion paper, *DiNunno et al.* [2002] will present a detailed examination of how the precursor data relate to the ozone budget for the CENP region.

2. Database

[7] The CENP region has been defined here as being bound on the west by the international dateline, on the east by the west coast of North America, and on the south by the equator. The northern limit has been constrained by latitudes beyond which there is little or no aircraft data.

[8] As noted earlier, the species of primary interest in this study are O_3, CO, NO_x, and H_2O. Also examined from the perspective of their use as tracers will be the nonmethane hydrocarbon (NMHC) species C_3H_8 and C_2H_2. The former species are critical to defining the photochemical environment within the CENP. But they also represent species for which there is a long history of successful observations.

[9] In this analysis, data components from ten different aircraft programs have been assembled. The selection of individual programs to contribute to the ensemble was determined based on a program providing observations of at least 3 of the 4 critical species: O_3, CO, NO, and H_2O. Table 1 lists these field studies along with further detail concerning the principal investigator associated with the data collection. It will be noticed that seven out of the ten field programs listed are associated with NASA's Global Tropospheric Experiment (GTE) program. Starting with the CITE studies, the NASA GTE program has provided a forum for the rigorous intercomparison of field measurement techniques [*Hoell et al.*, 1985, 1987a, 1987b; *Gregory et al.*, 1990]. Even though the data for this study have been taken from 10 different airborne campaigns, we believe the credibility of these measurements to be high, in that nearly all involved a CITE certified technique.

[10] The data from the ten field programs used in our analysis have been subdivided into two seasons, spring (March/April/May) and fall (September/October/November), reflecting the fact that nearly 85% of the available airborne data have been recorded during these two seasons. Table 2 provides the temporal distribution and scope of each program. It can be seen that the chronological period covered spans 1978 to 1999. The geographical range of each program is shown in Figure 2. Note, only those portions of individual flight tracks providing data for the ensemble are shown.

[11] The current compilation includes data also presented by *Emmons et al.* [2000], but has been expanded to include the GAMETAG data, the more recent PEM-Tropics B database, as well as the fall data recorded during the ACE 1 field study. Still another difference from Emmons et al. is that the current compilation focuses specifically on trends within the CENP region, as opposed to the focus of the work in

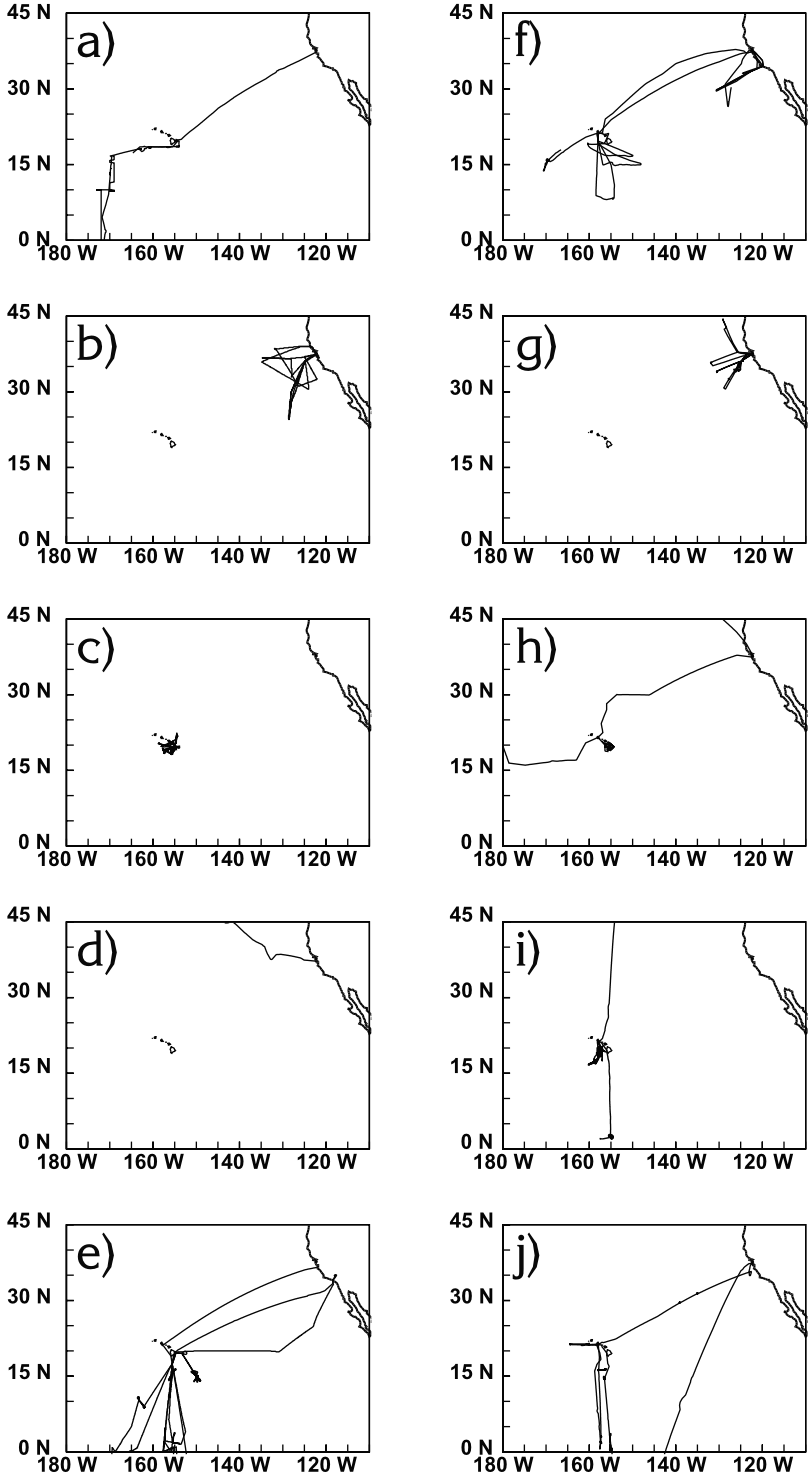

Figure 2. Flight tracks from field programs used in assembling airborne ensemble database. Lines represent portions of individual flights used in database. Left column figures represent flight programs flown during spring, right column were during fall. (a) GAMETAG, 1978; (b) CITE 1C, 1984; (c) MLOPEX II, 1992; (d) PEM-West B, 1994; (e) PEM-Tropics B, 1999; (f) CITE 1B, 1983; (g) CITE 2, 1986; (h) PEM-West A, 1991; (i) ACE 1, 1995; (j) PEM-Tropics A, 1996.

Emmons et al., a global database for comparison with global 3-D models and ozonesondes. Thus, while Emmons et al. make some comparisons to ozonesonde data within the CENP region, the global scope of their paper precluded it from providing a detailed analysis of this region. As a result, no detailed meteorological framework was provided for understanding the distribution patterns for species associated with any specific region such as that defined by CENP.

[12] For purposes of generating a more user friendly data set, temporal adjustments were made to a few of the

Table 1. Data Source: Investigators and Measurement Methods Employed

Species	Investigator	Method	Reference
	GAMETAG (*April–May 1978*)		
O_3	Davis and Delany	Chemiluminescence and UV absorption	A
CO	Heidt	Gas chromatography	B
H_2O	NCAR and Davis	chilled mirror hygrometer	C
	CITE 1B (*November 1983*)		
O_3	Gregory	Chemiluminescence and UV absorption	D
CO	Sachse	Laser differential absorption	E, F
NO	Carroll and Ridley	Chemiluminescence	G, H, I
	Torres	Chemiluminescence	
	Davis	Two-photon LIF	
H_2O	NASA-Ames	chilled mirror hygrometer	D
	CITE 1C (*April–May 1984*)		
O_3	Gregory	Chemiluminescence and UV absorption	D
CO	Sachse	Laser differential absorption	E, F
NO	Carroll and Ridley	Chemiluminescence	G, H
	Torres	Chemiluminescence	
H_2O	NASA-Ames	chilled mirror hygrometer	D
	CITE 2 (*August 1986*)		
O_3	Gregory	Chemiluminescence and UV absorption	J
CO	Condon	Grab sample, gas chromatography	J
NO	Carroll and Ridley	Chemiluminescence	K, L, M
	Torres	Chemiluminescence	
	Davis	Two-photon LIF	
H_2O	Beck	chilled mirror hygrometer	J
Hydrocarbons	Singh	Grab sample, gas chromatography	J
	PEM-West A (*September–October 1991*)		
O_3	Gregory	Chemiluminescence and UV absorption	N
CO	Sachse	Tunable Diode Laser	N
NO	Bradshaw	Two-photon LIF	N, O
	Kondo	Chemiluminescence	
H_2O	NASA-Ames	chilled mirror hygrometer	N
Hydrocarbons	Rowland	Grab sample, gas chromatography	P
	MLOPEX II (*April–May 1992*)		
O_3	Walega and Ridley	Chemiluminescence	Q
CO	Kok	TECO Gas correlation analyzer	Q
H_2O	mission	chilled mirror hygrometer	Q
	PEM-West B (*March 1994*)		
O_3	Gregory	Chemiluminescence and UV absorption	R
CO	Sachse	Tunable Diode Laser	R
NO	Bradshaw/Sandholm	Two-photon LIF	S, T
	Kondo	Chemiluminescence	
H_2O	DC-8 Aircraft	Frost point hygrometer	R
Hydrocarbons	Rowland/Blake	Grab sample, gas chromatography	U
	ACE 1 (*November 1995*)		
O_3	Kok	Chemiluminescence and UV absorption	V
CO	Kok	TECO Gas correlation analyzer	X
NO	Bradshaw	Chemiluminescence	V
H_2O	RAF-NCAR	chilled mirror hygrometer	V
Hydrocarbons	Blake/Rowland	Grab sample, gas chromatography	Y
	PEM-Tropics A (*August–October 1996*)		
O_3	Gregory (DC-8)	Chemiluminescence and UV absorption	Z
	Carrol (P3-B)	Chemiluminescence	
CO	Sachse	Tunable Diode Laser	AA
NO	Bradshaw (DC-8)	Two-photon LIF	Z
	Carrol (P3-B)	Chemiluminescence	
H_2O	DC-8 system (DC-8)	Chilled mirror hygrometer	Z
	Barrick (P3-B)		
Hydrocarbons	Blake	Grab sample, gas chromatography	AB
	PEM-Tropics B (*March–April 1999*)		
O_3	Gregory (P3-B & DC-8)	Chemiluminescence and UV absorption	AC
	Ridley (P3-B)	Chemiluminescence	
CO	Sachse	Tunable Diode Laser	AC
NO	Sandholm (DC-8)	Two-photon LIF	AC
	Ridley (P3-B)	Chemiluminescence	
H_2O	DC-8 system (DC-8)	Chilled mirror hygrometer	AC
	Barrick (P3-B)		
Hydrocarbons	Blake	Grab sample, gas chromatography	AD

References: A—*Routhier et al.*, 1980; B—*Heidt et al.*, 1980; C—*Routhier and Davis*, 1980; D—*Beck et al.*, 1987; E—*Sachse et al.*, 1987; F—*Hoell et al.*, 1987b; G—*Hoell et al.*, 1987a; H—*Ridley et al.*, 1987; I—*Davis et al.*, 1987; J—*Hoell et al.*, 1990; K—*Gregory et al.*, 1990; L—*Sandholm et al.*, 1990; M—*Carroll et al.*, 1990; N—*Hoell et al.*, 1996; O—*Kondo et al.*, 1996; P—*Blake et al.*, 1996; Q—*Atlas and Ridley*, 1996; R—*Hoell et al.*, 1997; S—*Sandholm et al.*, 1997; T—*Kondo et al.*, 1997; U—*Blake et al.*, 1997; V—*Bates et al.*, 1998; X—*Kok et al.*, 1998; Y—*Blake et al.*, 1999b; Z—*Hoell et al.*, 1999; AA—*Pougatchev et al.*, 1999; AB—*Blake et al.*, 1999a; AC—*Raper et al.*, 2001; AD—*Blake et al.*, 2001.

airborne databases. All measurements were merged into 1-min timelines. Thus, 1 min of GAMETAG data counts the same as 1 min of data recorded during PEM-Tropics B. But it also means that if a given measurement technique had a time resolution listed as 3 min, the same average value was used for three consecutive 1-min time periods. It should be noted, however, that observations of H_2O, O_3, CO, and NO were, for the vast majority of the data, reported at time resolutions of less than 10 seconds s.

[13] Table 2 lists the number of 1-min data points that were extracted from each field program. A data point here is classified as a 1-min sampling time period where at least one key species (O_3, CO, NO, H_2O) was measured. Recall, that another criterion for the acceptance of a data point was that, on a given flight, three out of the four critical parameters had to be measured. For 97% of the data points, at least two of the four critical species were recorded simultaneously; and for 74% of the points, three out of four variables were recorded. The above cited 1-min averaged observations, given the operational speed of the aircraft, typically covered a distance of 5+ miles. Thus, each 1-min sample can be viewed as sampling independent air parcels even though in many cases similarities appear from measurement to measurement as a result of the sampling occurring in a uniform air mass.

[14] Once all data filtering was completed, the ensemble data set was subdivided according to season, latitude, and altitude. The data was split into latitude bins of 5 degrees, and altitude bins of 1 km. Longitudinal homogeneity from 180° to 120°W was an initial assumption of our method, however, tests for this assumption are discussed later on in

Table 2. Airborne Ensemble Database Field Programs

Mission[a]	Time	No. of points[b]			
		H_2O	O_3	CO	NO
GAMETAG	April–May 1978	1815	1789	1147	0
CITE 1C	April–May 1984	596	596	596	395
MLOPEX II	April–May 1992	2166	1927	1259	0
PEM-West B	March 1994	172	176	171	171
PEM-Tropics B	March–April 1999	5052	4970	4433	2706
CITE 1B	November 1983	1235	1754	1024	666
CITE 2	August 1986	1382	1339	824	800
PEM-West A	September–October 1991	934	936	778	422
ACE 1	November 1995	1810	1521	1255	523
PEM-Tropics A	August–October 1996	3147	2446	2643	785

[a] Field programs included in the spring ensemble are in the left-hand column; those in the fall ensemble are in the right-hand column.
[b] The number of 1-min data points recorded during each program is cited.

the text (see e.g., precursor trends). Further analyses using these data were based on the median values estimated for each latitude/altitude bin. For bins that contained fewer than 5 data points, the mean value was used instead of the median. To establish that some of the less robust data bins did not have a distorting effect on the overall distribution for a given chemical variable, tests were carried out in which the distribution was plotted both with and without these data bins. This exercise is illustrated here for the case of ozone. For example, shown in Figure 3a is springtime ozone using all data bins. By contrast, Figure 3b represents the same ozone distribution plot but with all data bins containing fewer than 20 min of data having been removed. In this case, while individual features are slightly different with the removed cells, the broad patterns are still clearly evident. For this reason when discussing the data ensemble, we will limit our discussion to these broad patterns. Similar results are evident in Figure 4 for the fall ozone data, the broad patterns in the ozone distribution are anchored in data bins having extensive data. Examined, but not shown, were similar treatments for other critical species, which also showed that the broad patterns were not affected by the removal of less robust cells.

3. Meteorological Background

3.1. Streamlines

[15] Seasonally averaged streamlines and mean wind vectors at four different pressure levels are plotted in Figures 5 and 6 The streamline and mean wind field results for the Pacific basin reflect NCEP (National Centers for Environmental Prediction) data covering the years 1948–1999. The atmospheric pressure levels of 300, 500, 850, and 925 mb have been labeled in the text as: upper tropospheric (UT), middle tropospheric (MT), buffer layer (BuL) [see *Russell et al.*, 1998], and boundary layer (BL). These streamlines and wind fields allow for the discussion of large scale transport features, however, there is considerable variation in the pattern during each individual year.

[16] For the middle and upper troposphere, the spring and fall seasons can be differentiated in several ways. For example, during spring the shift from westerlies to easterlies typically occurs between 5° and 10°N; whereas, for fall it is 10°–20°. Another clear feature is the location of the upper tropospheric high pressure center in the Western Pacific which can have a significant impact on the distribution of photochemical species in the CENP region. In the spring, this system is centered over the Philippines (~15°N, 125°E), in the fall it shifts to the east/northeast to 25°N and 160°E. The net effect is that transport to the eastern North Pacific in the fall takes a rather circuitous path, while in the spring it follows a more zonal and direct path. From 15° to 30°N, the spring flow is also much faster in the western Pacific. This combination of factors leads to a reduction in the travel time for crossing the North Pacific at high altitudes during spring.

[17] As shown in Figure 6, the general transport features for the BL and BuL are quite similar between fall and spring. The main difference is in the velocity of the flow. In the spring it is about 20% more intense, with average velocities in excess of 10 m/s at 850 mb for latitudes $\geq$40°N. For the eastern tropical North Pacific, the situation is nearly reversed, stronger winds occur in the fall, rather than spring, over the pressure range of 850 mb and below. However, the spring season sees a stronger northerly component to the flow in the eastern tropical North Pacific. This stronger northerly component in spring increases the likelihood of North American emissions reaching the eastern tropical Pacific. By contrast, in the fall season the steady easterly tropical flow tends to provide a Central/South American influence on the tropical eastern North Pacific.

[18] Since the broad flow patterns cited above will be used to discuss geographical/altitudinal trends in photochemical precursor species, we have found it useful to define three latitudinal zones in the text: tropical (0°–15°N), transition (15°–30°N), and midlatitude (30°–45°N). These divisions generally apply to pressure altitudes corresponding to less than 300 mb. The tropical zone is defined here as that region typically under the control of easterly flow during both seasons of the year. The transition zone is characterized by shifting flow patterns that are a function of both altitude and season. The transition from easterlies to westerlies typically occurs over the 15°–30°N latitude range, with the changeover taking place at the northern extreme during fall. The midlatitude zone is controlled by westerly flow in both seasons, but experiences faster transport during spring.

3.2. Lightning Climatology

[19] Lightning is clearly one of the more important sources of NO_x in the Pacific [*Goldenbaum and Dickerson*, 1993; *Pradeep Kumar et al.*, 1995; *Levy et al.*, 1996]. Thus,

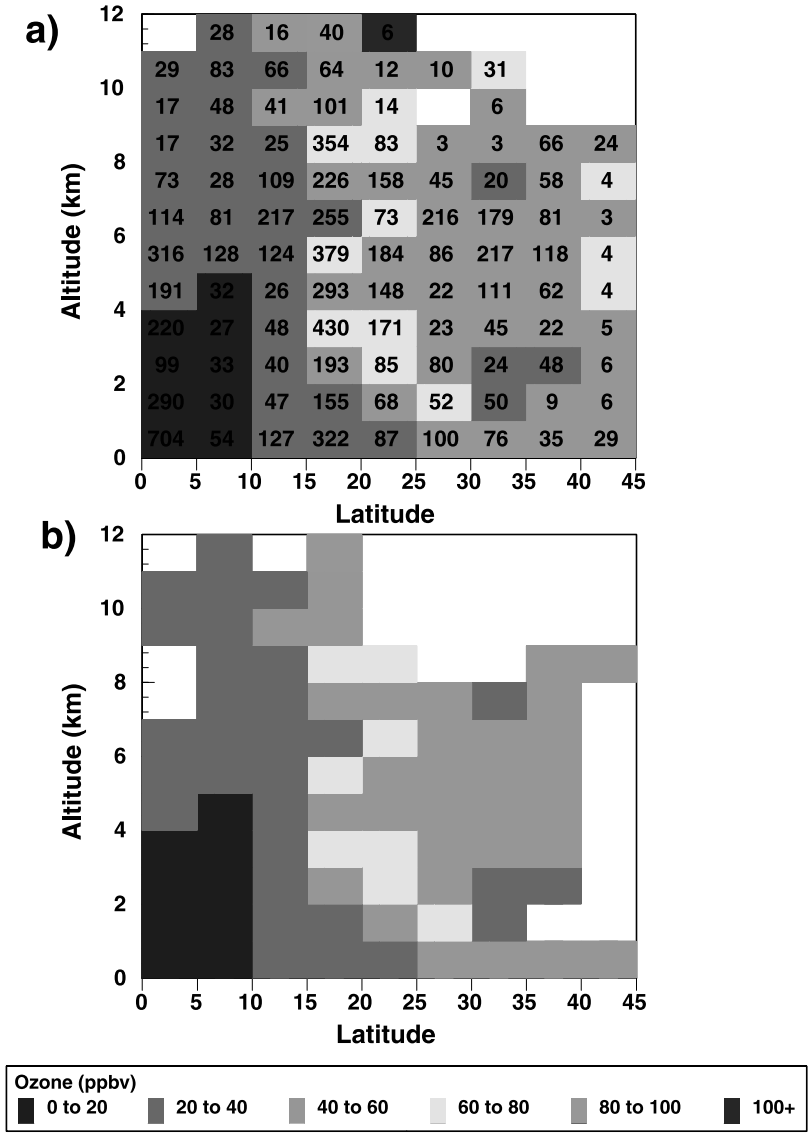

Figure 3. Low altitude, long-term seasonal climatologies for streamlines and wind speeds in the Northern Pacific basin. Profiles were generated using averaged NCEP reanalysis products from 1948 to 1999. Streamlines are in red, wind speed, and direction are represented by black arrows at 850 and 925 mb pressure levels. CENP region is enclosed in grey box. (a) spring, 850 mb; (b) fall, 850 mb; (c) spring, 925 mb; (d) fall, 925 mb. See color version of this figure at back of this issue.

the distribution of lightning, and its seasonal variations in the Pacific is of considerable interest in determining the CENP region's chemical climatology for NO_x. High resolution lightning data has been available since the spring of 1995 based on NASA's new Optical Transient Detector system [*Christian et al.*, 1989]. Because of this system's capability of providing seasonally resolved data in a single year, it has proven quite useful in examining the patterns of lightning over the Pacific basin.

[20] As related to CENP, four key areas require examination. These include land areas over eastern/southeastern Asia, the western Pacific region, land areas over Central America/northern South America, and the CENP region itself. Lightning flash data recorded during PEM-Tropics A (fall, 1996) and PEM-Tropics B (spring, 1999) are those shown in Figures 7a and 7b. Although variations in lightning patterns do occur from year to year, these two years appear to be broadly representative of the lightning patterns for the seasons selected given the 5 years of high resolution data. For the fall, of the regions cited, of particular interest is the lightning flash density shown for Asia and the western Pacific. It is this large region just upwind of CENP that has the largest impact when the prevailing wind is westerly as previously discussed by *Davis et al.* [1996] and *Crawford et al.* [1997a, 1997b]. In addition, the convection associated with this lightning potentially could serve to move land-based surface NO_x pollution to the upper atmosphere, thus providing yet another high altitude source of this species. As shown in Figure 7, widespread lightning is detected over Southeast Asia during both spring and fall, with the highest intensity occurring during spring. Similarly, the highest lightning flash density is also seen over China during the spring. This seasonal pattern is reversed when examining the western Pacific (0°–45°N, 120°–180°E). During the fall it is

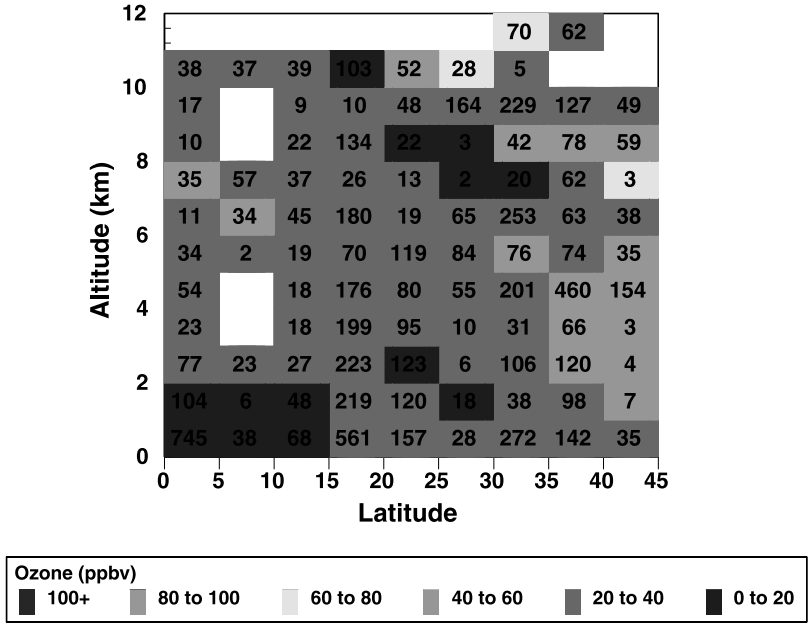

Figure 4. Seasonal lightning frequency data recorded by NASA's Optical Transient Detector. Units are number of flashes per three month season. CENP region is enclosed by outline. (a) Fall, 1996 (time period for PEM-Tropics A); (b) Spring, 1999 (time period of PEM-Tropics B). See color version of this figure at back of this issue.

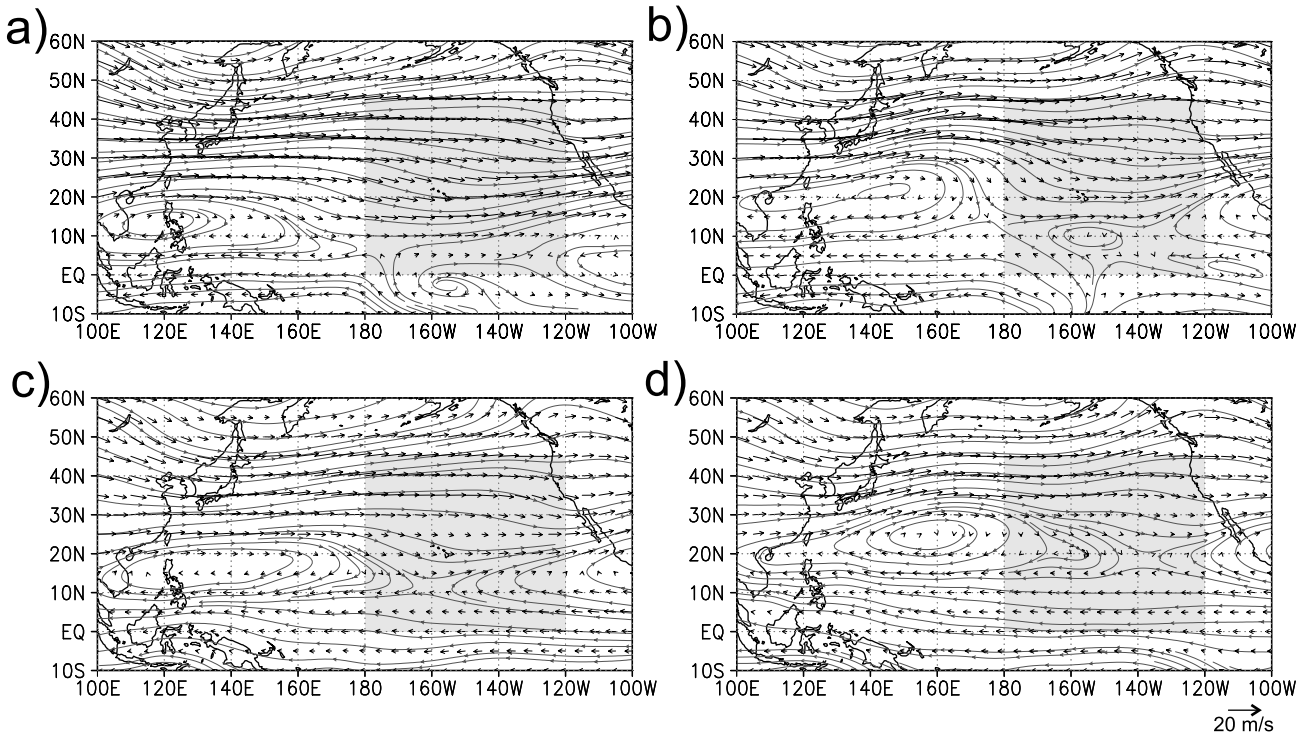

Figure 5. Seasonal altitudinal/latitudinal photochemical precursor distributions derived from airborne ensemble database. Data is segregated into 5 degree latitude and 1 km altitude bins. Values plotted are medians for: (a) O_3, spring; (b) O_3, fall; (c) CO, spring; (d) CO, fall; (e) NO_x, spring; (f) NO_x, fall. NO_x values were generated using observed NO and model generated NO_2. See color version of this figure at back of this issue.

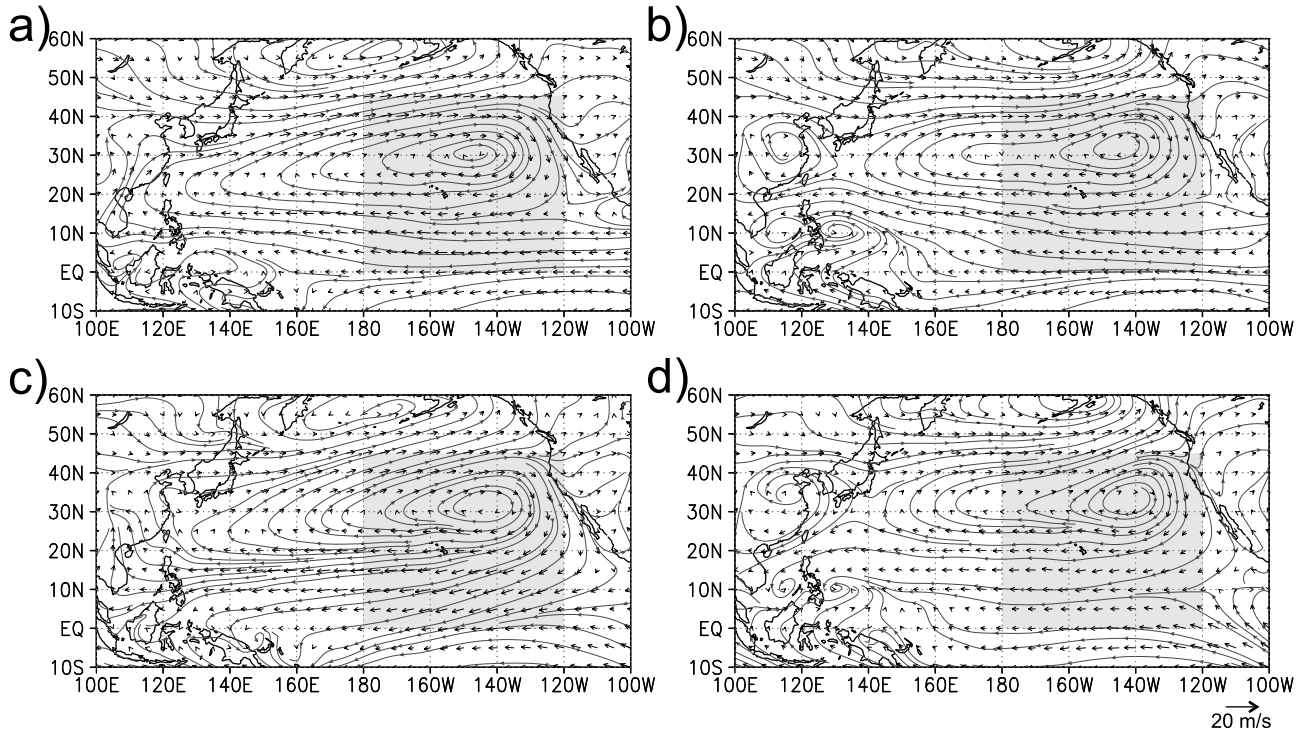

Figure 6. Comparison of ozonesonde data from Hilo, Hawaii [*Logan*, 1999] with CENP airborne O_3 database. (a) spring; (b) fall. See color version of this figure at back of this issue.

greater, but this flash rate is still small when compared with that over the Asian continent. However, since the transport time to the CENP region is shorter, the possibility of western Pacific lightning influencing the CENP region is still high. Figure 7a also reveals that the lightning flash density over Central America/northern South America has a distinct seasonality to it, peaking during the fall wet season.

[21] Within the CENP region itself, one of the major seasonal differences is that the central North Pacific during fall has a substantially higher flash rate than for spring. On the other hand, for the tropical eastern North Pacific, the spring flash rate that extends out from the central American coast is seen elevated over that for fall.

3.3. Precursor Trends

[22] Precursor trends will be examined as a function of season, latitude, and altitude. Any discussion of latitudinal trends will be further guided by the earlier meteorological discussion and thus will focus on the latitudinal divisions of tropical, transition, and midlatitude zones. After contrasting the two seasonal data sets, comparisons will be made with any available ground-based, sonde, and/or satellite observations. The latter data will also be used to explore possible longitudinal trends in the precursor data as well as to assess possible long-term temporal trends for a species.

3.4. Ozone

[23] The springtime distributions in ozone are those shown in Figure 8a. For the tropical BL, values are typically in the range of 0–20 ppbv. Tropical values are seen increasing modestly with altitude, where levels of 20–40 ppbv are reached between 5 and 12 km. Shifting to the transition zone (15°–30°N), higher values are seen at virtually all altitudes. However, a significant gradient can be seen even within the BL transition zone where values range from 20 to 60 ppbv, the northern end being higher. This follows from the climatological flow patterns shown in Figure 6c where increasing westerly flow, and midlatitudinal influence, is evident with increasing latitude. In addition, a greater influx of ozone occurs from stratospheric intrusions at these higher latitudes. This is particularly the case for ozone in spring, when the stratospheric influence is greater [*Wang et al.*, 1998] At still higher altitudes (2–10 km) within the transition zone, ozone again shifts to higher values. These values are maintained across the transition zone, and typically lie between 40 and 80 ppbv. Recall, middle and upper free tropospheric flow during the spring shifts from easterly to westerly at ~12°N. This places the free tropospheric transition zone firmly under the influence of outflow from Eurasia. Midlatitude (30°–45°N) ozone values are seen as being quite similar to those in the transition zone. BL values range from 40 to 60 ppbv, increasing to 40–80 ppbv at free tropospheric altitudes. Of the three zones examined, the midlatitude zone shows the smallest shifts in concentration with altitude, reflecting the continuity in westerly flow seen at nearly all altitudes.

[24] As shown in Figure 8b, the fall pattern for ozone is quite different from that for spring. In the tropics BL values of 0–20 ppbv increase to 20–40 ppbv in the middle and upper troposphere. Quite significant is the absence of large latitudinal gradients in the tropics and transition zones, particularly at higher altitudes. In fact, there is very little gradient in the transition zone even as a function of altitude. The transition zone BL experiences northeasterly flow

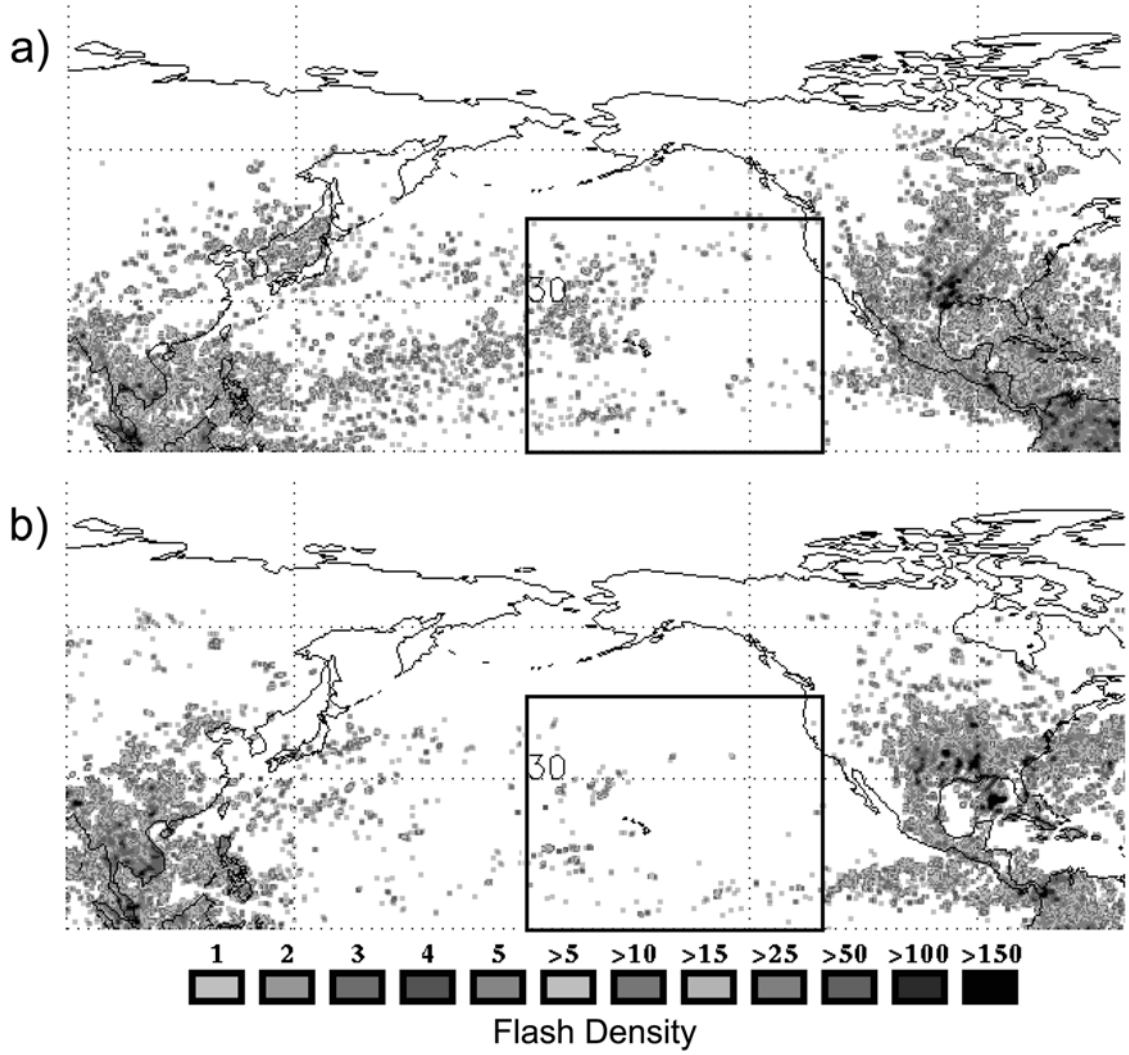

Figure 7. Long-term monthly median observations of CO recorded in the CENP region by the Climate Monitoring and Diagnostics Laboratory. a) SHM, Shemya Island, 52°N, 173°E; and MID, Midway Island, 28°N, 177°W; b) MLO, Mauna Loa, 19°N, 155°W, 3.3 km; and KUM, Cape Kumakahi, 19°N 154°W; and c) CHR, Christmas Island, 2°N 157°W. Note, all stations except for Mauna Loa are below 50 m in altitude. See color version of this figure at back of this issue.

during the fall at the 925 mb level, and therefore is also influenced by the air from the midlatitude BL. Both of these zones show ozone concentrations in the 20–40 ppbv range. At free tropospheric altitudes, however, the midlatitude picture shifts, and it can be seen that significant increases in ozone are present over that observed in the tropics and the transition zone. The free troposphere at these latitudes is under a westerly flow regime, and ozone values frequently reach the 40–60 ppbv range. Thus, one of the biggest latitudinal transitions that occurs in the free troposphere during fall occurs north of 30°N, with the transition zone looks more like the tropics.

[25] A comparison of the spring and fall patterns indicates that the difference is primarily seen in the transition and midlatitude zones. In the free troposphere, the typical ozone value is 15–30 ppbv higher in spring than fall. The transition zone, however, experiences the largest shift, reflecting the large change in flow patterns for this zone between spring and fall. Within the BL, ozone levels are also seen as higher in spring, especially at midlatitudes. For example, the 20–40 ppbv shown for fall typically shifts to the 40–60 ppbv range during spring.

[26] Data from ground-based stations such as that from Mauna Loa Observatory (19.5°N, 115.6°W, 3.4 km) provide an excellent opportunity to examine long-term trends in North Pacific ozone. Such data can also serve as a basis for exploring inter-annual variability. For Mauna Loa, the data reveal an insignificantly small increase in ozone over the time period of 1973–1992 [*Oltmans and Levy*, 1994], with a statistically insignificant difference between spring and fall, e.g., 0.55% versus 0.04%, respectively.

[27] Yet another interesting comparison is that between the airborne data and profiles generated from ozonesonde data. The most important of these for the CENP region are those launched from Hilo, Hawaii (~20°N). The data from Hilo involves launches covering the time period of 1985 to 1993, as analyzed and reported by *Oltmans et al.* [1996] and *Logan* [1999]. As shown in Figure 9, the average profile

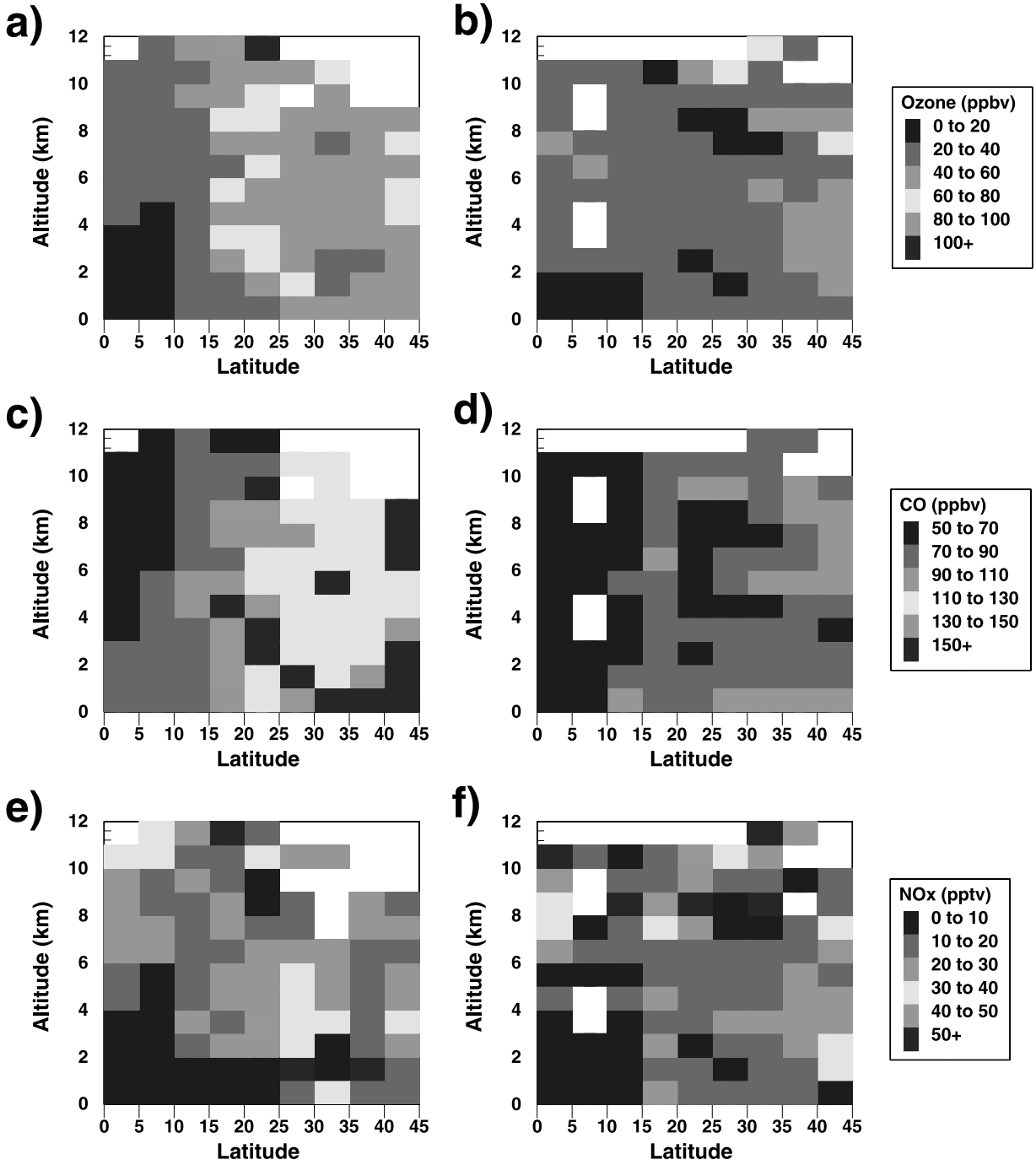

Figure 8. Multiyear airborne observations of free tropospheric CO (>2 km) as a function of distance from USA west coast. Box and whisker plot showing median, inner quartiles, and 5%/95% values for: (a) spring; (b) fall. See color version of this figure at back of this issue.

derived from the spring and fall sonde data matches up reasonably well (especially below 700 mb) with the median values from the aircraft data that bracket Hilo in latitude. In particular, as seen in the airborne data, a spring maximum (e.g., >60 ppbv, 700–300 mb) is evident in the sonde data. A more detailed analysis reveals that the spring airborne data, on average, is within 5 ppbv of the sonde results for altitudes below 700 mb; but is 5–20 ppbv lower than the sonde values in the 700–300 mb altitude range. For fall, the airborne data are 5–10 ppbv higher than the sonde profile in the lower free troposphere and 5–15 ppbv lower than the sonde profile in the upper free troposphere.

[28] A final comparison with the aircraft data is that provided by the availability of TOMS and SBUV satellite data [*Fishman et al.*, 1990]. The derived tropospheric column ozone values span the time period of 1979–1998, thus overlapping nearly perfectly the time period of the aircraft observations. An interesting feature of the satellite data is that it affords the opportunity to examine latitudinal as well as longitudinal trends in North Pacific ozone. In

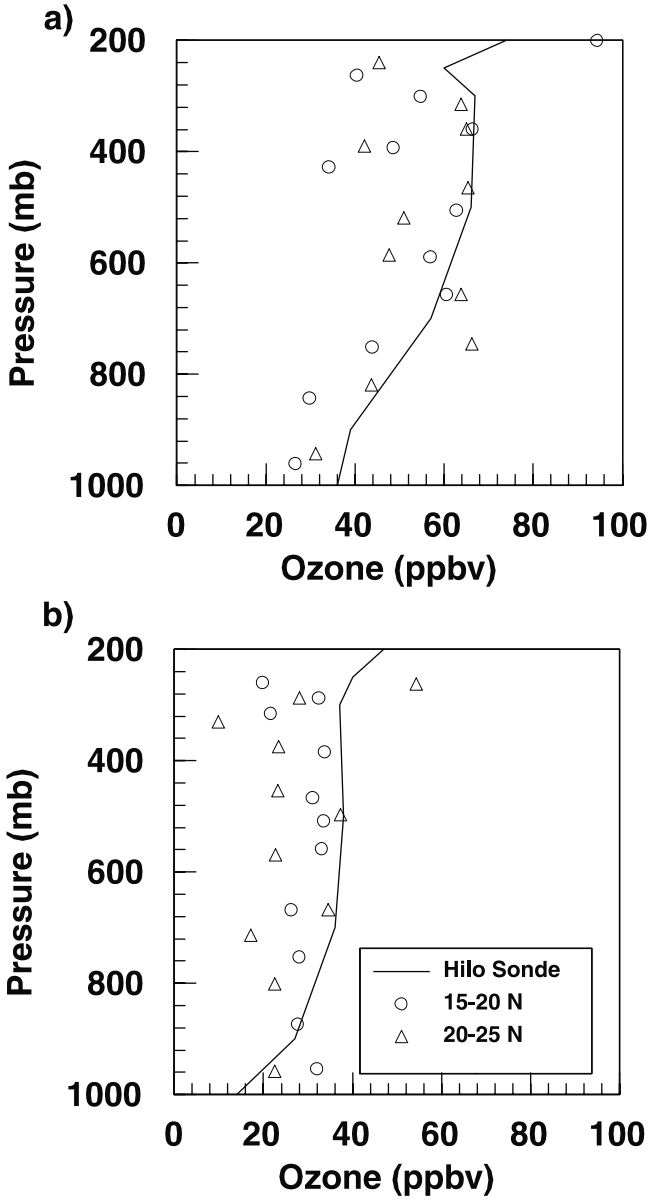

Figure 9. Seasonal altitudinal/latitudinal photochemical precursor distributions derived from airborne ensemble database. Data is segregated into 5 degree latitude and 1 km altitude bins. Values are plotted for (a) spring ozone, all grid cells. Number of 1-min observations labeled for each grid; (b) spring ozone, grid cells with 20+ min of data.

particular, the satellite derived longitudinal picture allows for a further assessment of the representativeness of the aircraft data for the CENP region since the latter was far more limited in its geographical coverage.

[29] From the TOMS/SBUV analysis, the clearest longitudinal trend that emerges is that shown in Table 3 which reveals lower total column ozone in the central Pacific relative to the eastern Pacific. This difference is reflected in the two independent values derived for column ozone: 180°–150°W versus 150°–120°W. This comparison shows that for midlatitudes there is very little variation between the two. However, for both spring and fall, the transition zone in the eastern Pacific is seen as having 5–10% higher column ozone than for the central Pacific. This 10% higher value is maintained as one moves to the tropical zone during fall, and increases to ~30% for spring. These higher values during spring may be due to more northerly flow in this region versus the central Pacific, and/or to a seasonal biomass burning influence from Central and northern South America [*Sanhueza*, 1991; *Hao and Liu*, 1994]. Overall, however, the differences are not overwhelming, and thus, they would tend to confirm the reasonableness of our assumption of longitudinal uniformity in constructing the airborne databases.

[30] If each of the aircraft data zones is averaged over all longitudes and then compared to the corresponding average derived from satellite data, the level of agreement is found to be quite good for two zones but only moderate for the third. These results are shown in Table 4. For the tropical zones, agreement between the airborne estimates and the residual method is good for both seasons. This agreement continues to be strong for the springtime transition zone, but the value from the residual method far exceeds that for the aircraft ensemble in fall. This discrepancy, with the tropospheric residual being higher than the ensemble, continues for both seasons in the midlatitude zone. The fact that all comparisons reveal lower values when using the ensemble aircraft data might suggest the presence of a systematic error in one or both of the sampling approaches, but at this time, no details concerning such possible errors are available.

3.5. Carbon Monoxide

[31] The latitudinal/altitudinal airborne CO profiles for the spring time period are shown in Figure 8c. BL/BuL (<3 km) values in the tropical zone are seen ranging from 70 to 90 ppbv. Only a modest decrease is seen in the values for this zone with increasing altitude. As one moves northward into the transition zone CO is seen to increase significantly, with BL values ranging from 90 to 150+ ppbv. Free tropospheric values in this zone also reveal elevated values with most of the data ranging from 110 to 150+ ppbv. Recall, this latitudinal zone experiences significant Asian outflow in the spring. It is noteworthy, however, that these outflow periods can also be intermixed with periods of isolation, as detailed by *Hess et al.* [1996]. The midlatitude zone shows somewhat greater uniformity in CO, more typical values ranging between 110 and 130 ppbv, but with several altitude/latitude bins that exceed 150 ppbv.

[32] The fall CO data shown in Figure 8d reveal far more uniform and overall lower values as a function of altitude and latitude versus spring. This can be at least partially accounted for by the large drop in northern hemispheric CO values that occurs during the summer and typically continues into fall [*Novelli et al.*, 1998], reflecting large scale oxidation by OH. Also contributing to the reduction is the much weaker westerly flow at this time of year.

[33] Tropical CO values are seen as relatively uniform at all altitudes, 50–70 ppbv being the typical range. Further to the north in the transition zone, CO is somewhat elevated over that in the tropics with values from the BL and throughout most of the free troposphere typically ranging from 70 to 90 ppbv. On average, mixing ratios in the midlatitudes are somewhat elevated relative to the transition zone, the range being 70–110 ppbv.

Table 3. Seasonal Comparison of Tropospheric Ozone Column Residuals Derived From SAGE and TOMS Data [*Fishman and Brackett*, 1997]

	Spring[a]			Fall[a]		
Latitude	180°–150°W	150°–120°W	% Higher[b]	180°–150°W	150°–120°W	% Higher[b]
40–45	47.9	48.3	0.73	31.6	31.4	−0.63
35–40	38.8	41.6	7.35	31.3	32.9	5.11
30–35	34.0	37.0	8.81	31.6	34.4	8.70
25–30	33.3	34.9	4.81	31.2	33.6	7.69
20–25	32.9	34.4	4.41	28.3	30.4	7.42
15–20	30.1	33.3	10.63	24.4	26.6	8.79
10–15	25.8	30.8	19.19	21.1	23.5	11.37
5–10	22.3	28.4	27.07	18.5	20.6	11.35
0–5	20.4	26.8	31.37	16.6	18.1	9.04

[a] All ozone column values are in Dobson units.
[b] % Higher is the amount of increase in the Eastern Pacific over the Central Pacific.

[34] An examination of the fall flow patterns in the central Pacific (e.g., Figures 6b and 6d) indicate that in the transition zone, flow at BL and BuL altitudes tends to be northeasterly, thus transporting in higher latitude air into this zone with typically higher than average concentrations of CO. In contrast, at 500 mb (Figure 5d), the flow pattern is seen as being more variable, and overall weaker. Thus, under these conditions it is quite possible that the CO sampled may have undergone significant processing since leaving its continental source region. Flow at the 300 mb level (Figure 5b) is seen as shifted fully to the west, thus potentially providing air parcels that may have been influenced by deep convection over Asia and/or Europe.

[35] Contrasting the spring and fall CO airborne data reveals major differences at nearly all latitudes and altitudes. The largest difference is seen occurring for the transition and midlatitude zones where free tropospheric mixing ratios drop from the 110–150+ range to 70–110 ppbv. While spring for both the transition and midlatitude zones shows a distinct trend toward strong westerly flow, this flow becomes much weaker in fall and overall, the pattern is less well defined. As noted above, the difference between seasons is also a product of there being reduced CO levels during the northern hemispheric summer [*Novelli et al.*, 1992, 1998].

[36] At high altitudes, CO levels in the tropics is far less affected by the aforementioned seasonal factors, thus we see free tropospheric values tending to be quite similar for both seasons of the year (e.g., 50–70 ppbv). But below 4 km this is not true, and springtime values are shown as being nearly 20 ppbv higher than those observed in fall. During both seasons of the year, the tropical zone experiences converging easterly and northeasterly flow at the 850 and 925 mb levels, placing the main source region for this zone as Central America and northern South America. Biomass burning levels in Central and northern South America maximize in the March–May time period [*Sanhueza*, 1991; *Hao and Liu*, 1994]. In contrast, very little burning occurs during the September–November period. Considering the fact that biomass burning has been clearly linked to CO enhancements in other regions of the world [*Talbot et al.*, 1996; *Christopher et al.*, 1998; *Olson et al.*, 1999], it is quite likely that the cause of the seasonality in low altitude tropical CO levels is due to the above cited seasonal burning trends. In addition, the elevated concentrations of CO were not accompanied by elevations in nonmethane hydrocarbons (NMHC's) that would be expected from the more rapid transport associated with midlatitude influence. This further implies the transport of well-aged biomass burning emissions would be brought to the tropical CENP on the easterly trade winds.

[37] A 3-D model simulation of CO carried out by *Holloway et al.* [2000] provides supporting evidence of the likelihood that biomass burning is probably one of the larger contributing factors to the tropical seasonal CO difference. In this case, the simulation results for Christmas Island reproduced quite nicely the observed CO mixing ratios during spring, with modeled values showing a peak in April. While model input included source contributions from methane oxidation, anthropogenic fossil fuel emissions, biogenic hydrocarbon oxidation, and biomass burning, the spring increase was found to be primarily due to increased input from biomass burning.

[38] Ground based observational data also afford an opportunity for examining seasonal and inter-annual variability in CO. The now well established seasonal trend in the northern hemisphere, with maximum values occurring in late winter/early spring, and a minimum in summer [*Novelli et al.*, 1998] appears to be well reflected in the aircraft data. For the North Pacific, the ground-base data are shown in Figure 10. Quite clearly, the peak value in CO for stations at Christmas Island (2°N), Cape Kumukahi, HI (19.5°N), Mauna Loa, HI (19.5°N), Midway (28°N), and Shemya, AK (53°N) occurs during the month of March. A sharp drop in CO follows this peak month, with the minimum occurring in August. Year to year variations can also be signifi-

Table 4. Satellite- and Airborne-Derived Tropospheric Column Ozone for the CENP Region

	Spring			Fall		
Season Zone	Tropical	Transition	Midlatitude	Tropical	Transition	Midlatitude
Aircraft Ensemble	22.6	37.3	33.0	21.2	20.1	22.6
Trop. Residual	22.5	38.3	40.4	19.7	29.3	32.2

All numbers are in Dobson units.

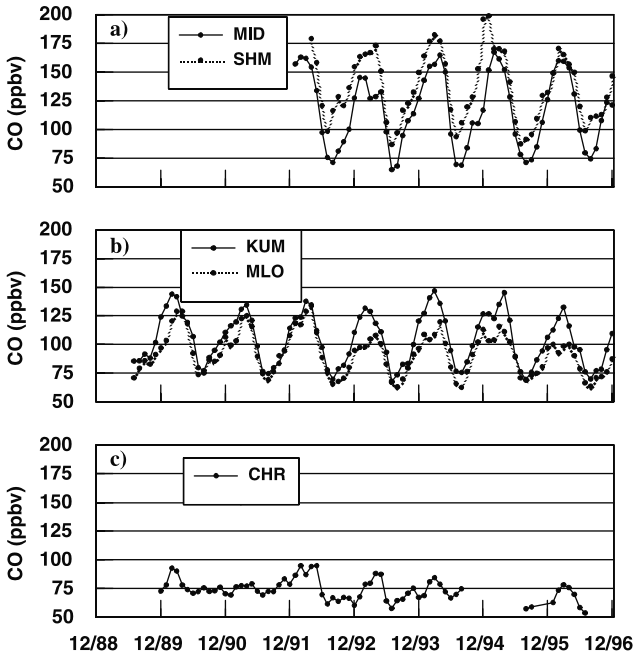

Figure 10. Seasonal altitudinal/latitudinal photochemical precursor distributions derived from airborne ensemble database. Data is segregated into 5 degree latitude and 1 km altitude bins. Values are plotted for fall ozone, all grid cells. Number of 1-min observations labeled for each grid.

cant. One of the largest of these can be seen in the data from Mauna Loa. The peak to peak decrease between April 1992 and April 1993 is 20%.

[39] Possible long-term trends in CO may also be raised as an issue when looking at the 20 year integrated record of aircraft data. Implicit in our method of combining various aircraft field studies is the assumption that any significant long-term temporal trend would be small. In the case of CO in the northern hemisphere, only a 1% increase per year was observed prior to 1990 [*Khalil and Rasmussen*, 1984, 1988]. This trend was then reversed, with an ~2% decrease occurring over the time period of 1991–1996 [*Novelli et al.*, 1998; *Khalil and Rasmussen*, 1994]. Thus, overall the shifts in CO over the 20 year period of airborne data collection have been very modest.

[40] As for ozone, the issue of longitudinal representativeness in the CO airborne database can be explored using space platform generated data. The database in this case is that which has been provided by NASA's Measurement of Air Pollution from Satellites (MAPS) instrument [*Reichle et al.*, 1986, 1990; *Connors et al.*, 1999]. These snapshot results are summarized in the form of Table 5. From here three tentative conclusions can be drawn: 1) the MAPS data, like the aircraft results, clearly shows evidence of a spring maximum in CO; 2) the 1984 versus 1994 fall MAPS data suggest that CO snapshots can produce considerable variability even within one season, and 3) as related to longitudinal gradients, the MAPS data suggests that the largest variations in CO occur in the southeastern section of the CENP region (e.g., 0°–20°N, 120°–150°W) during fall. Expanding on this third point, the tropical eastern Pacific (120°–150°W) consistently shows higher levels of CO than does the tropical central Pacific (150°–180°W), particularly when examining the 1984 data. Recall, that based on the earlier meteorological wind field/streamline maps, this region is primarily influenced by northerly winds at low altitudes and easterly winds at high altitudes. Thus, the higher CO values seen in this sector are likely indicative of recent continental influences.

[41] Limiting the MAPS data to the transition and midlatitude zones, there appears to be a minimal gradient in CO when comparing the central versus the eastern Pacific. Further evidence supporting this longitudinal continuity in CO can be seen in the aircraft observations where the CO data shown in Figure 11 have been binned according to longitude as a function of distance from the North American continent. This box and whisker plot covers the range of 5 to 2000 km from the coast of North America and the free tropospheric altitude range of 2–10 km. The resulting median values from these binned data show only a modest trend of increasing values as the USA coast is approached. This would suggest that the influence of local pollution on offshore North Pacific levels of CO at latitudes north of 20°N is minimal. Based on trajectory analysis and CO sampled from Mauna Loa and other Pacific islands, *Jaffe et al.* [1997] reached a somewhat similar conclusion. Jaffe et al. also estimated that only 12% of the high CO events seen at Mauna Loa could be assigned as being due to transport from the North or

Table 5. Seasonal CO MAPS Data for the CENP Region [*Connors et al.*, 1999]

	Fall				Spring	
	OSTA3-1984		SRL2-1994		SRL1-1994	
Latitude	180°–150°W	150°–120°W	180°–150°W	150°–120°W	180°–150°W	150°–120°W
40–45	85.6	86.1	101.8	101.7	117.5	110.1
35–40	79.2	69.7	104.2	100.5	118.1	118.3
30–35	72.4	65.1	115.2	100.1	124.2	119.5
25–30	66.4	61.9	109.0	101.7	124.2	110.9
20–25	62.5	67.2	94.4	106.8	115.6	104.5
15–20	56.0	77.3	83.5	88.3	103.8	97.9
10–15	60.4	75.6	76.4	84.6	98.7	91.2
5–10	62.2	74.4	74.6	83.7	86.9	90.7
0–5	53.0	70.2	72.6	82.3	80.6	87.5

All values are in ppbv.

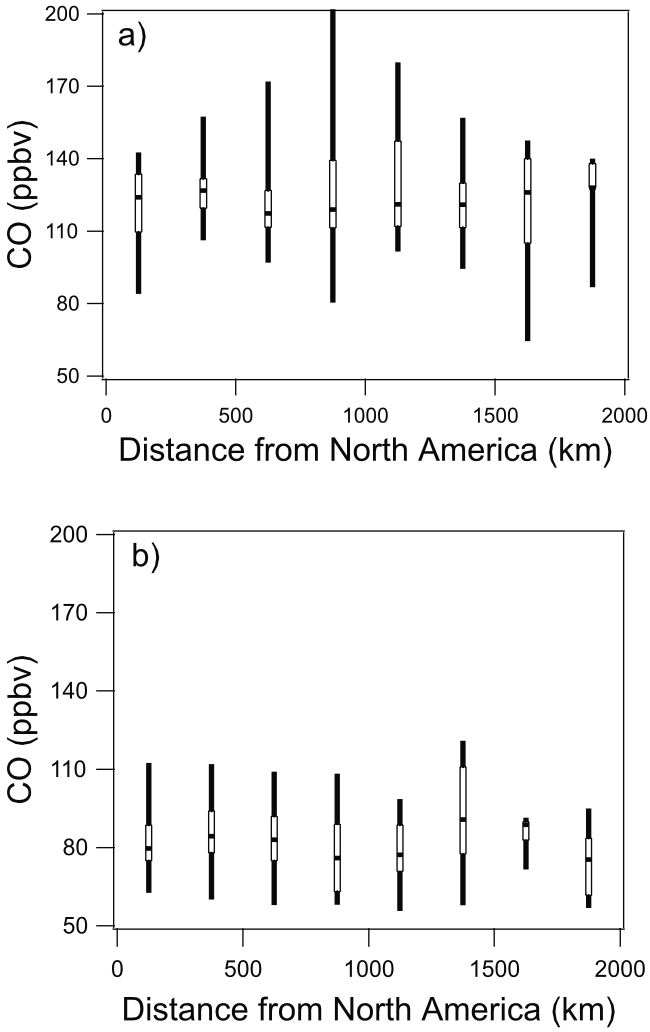

Figure 11. High altitude, long-term seasonal climatologies for streamlines and wind speeds in the Northern Pacific basin. Profiles were generated using averaged NCEP reanalysis products from 1948 to 1999. Streamlines are in red, wind speed and direction are represented by black arrows for 300 and 500 mb pressure levels. CENP region is enclosed by grey box. (a) spring (March, April, May), 300 mb; (b) fall (September, October, November), 300 mb; (c) spring, 500 mb; (d) fall, 500 mb.

Central American continents, as opposed to 59% of the cases being East Asian in origin.

3.6. Nitrogen Oxides

[42] Airborne generated profiles of NO_x are shown in Figures 8e and 8f. Because only NO data were available in most cases [*Bradshaw et al.*, 2000], the NO_x values shown were those estimated from model calculated NO_2 values [*Crawford et al.*, 1999; *Chen et al.*, 2001]. As shown in Figure 8e, the springtime levels of NO_x in the tropical zone increase from 0 to 10 pptv below 4 km to 10–40 pptv between 4 and 12 km. Given the relatively low concentrations of CO and O_3 observed concurrently, it would appear that these high altitude NO_x levels probably have a lightning source. Figure 8e indicates that the transition zone also has rather low BL and BuL NO_x values (0–10 pptv), but does display the occasional impact from a continental plume (e.g., see discussion later in text). Free tropospheric NO_x values for the transition zone reveal significant variability, with typical concentrations ranging between 20 and 40 pptv. This trend is seen continuing on into the midlatitudes.

[43] During the fall season (Figure 8f), the trend for all zones for all altitudes below 6 km is that of finding NO_x values that vary considerably but rarely exceed 30 pptv. At still higher altitudes, particularly for the tropical and transition zones, elevated NO_x (i.e., 30–50+ pptv) is quite evident and is most likely due to either local lightning or some combination of local lightning plus imported NO_x resulting from deep convection. The latter source would appear to have been over a marine area since the high NO_x values show no correspondence with either elevated CO or NMHC's. Moving to midlatitudes, the NO_x distribution is seen as quite variable across the entire altitude range, showing a mixing ratio range of 10–50+ pptv.

[44] A comparison of the spring and fall data reveals that for the tropical zone, NO_x levels for <6 km are quite similar and quite low, only occasionally exceeding 15 pptv. This appears to reflect two factors: the isolation of this tropical altitude regime from major sources and the short lifetime of NO_x. During PEM-West A, *Davis et al.* [1996] analyzed western tropical Pacific NO_x data and determined its lifetimes at low altitudes to range from 1 to 2 days. At tropical latitudes in the southern hemisphere (0°–10°S), *Schultz et al.* [1999] also concluded that low altitude NO_x had a lifetime of ~1 day. For the CENP region, *Moxim et al.* [1996] concluded from GCTM runs that 70–90% of tropical BL NO_x during the fall was the result of the decomposition of subsiding PAN. This contribution rose to 90+ % for spring.

[45] For the upper troposphere larger differences can be seen between the tropical spring and fall data. The fall time period shows far more high values. The longer lifetime of high altitude tropical NO_x (estimated at 2–6 days by *Davis et al.* [1996] based on PEM-West A data and 5–7 days by *Schultz et al.* [1999] using PEM-Tropics A observations) allows for transport from more distant sources. In addition, above 7 km the influence of lightning increases. For example, according to cloud model simulations by *Pickering et al.* [1998], for tropical marine environments the largest fraction of lightning generated NO is released between 7 and 13 km. The sporadic nature of lightning within this region could thus account for much of the high variability observed in the high altitude NO_x. As shown in Figure 7, lightning within the CENP region is enhanced during fall as compared to spring. Convection followed by long range transport of continental emissions is still another potential source. However, since much of the upper altitude fall tropical enhancement in NO_x was found not to be accompanied by elevations in CO or NMHC's, this suggests that the lightning was most likely over a marine region.

[46] While the data in Figure 7 indicate only modest differences between BL NO_x for spring versus fall, as related to the transition and midlatitude zones, there are some quite distinct differences in the lower free troposphere. NO_x in the transition zones was higher in spring than fall, with a typical range of 20–40 pptv versus 10–30 pptv, respectively. Given its relatively short lifetime, the more intense transport during the spring time period [*Merrill*, 1996] has the potential for enhancing NO_x. Evidence of

direct transport of NO_x from Asia was detected during PEM-West B, with factors of two and more being seen in elevated BL NO_x (20°–30°N) as far as 2000 km downwind of the Asian continent [*Crawford et al.*, 1997a]. However, the CENP region is approximately 4000–8000 km downwind of Asia. Thus, while some influence due to direct transport of NO_x might be expected, the additional travel time would seem to dampen the importance of this source. But the latter source assumes that all transport took place at low altitudes where, on average, NO_x has a shorter lifetime. An alternative to this source mechanism is the lofting of an air parcel to high altitude over land areas, long range transport, followed by subsidence.

[47] During springtime there is evidence that lofting, long range transport, followed by subsidence can lead to elevated low altitude NO_x levels in both the transition and midlatitude zones. In one case during PEM-tropics B, NO_x levels of >100 pptv were measured within the BuL (e.g., 28°N, 130°W at 1.3–1.9 km). These NO observations were accompanied by high HNO_3, elevated CO and NMHC's, and low dew points. Kinematic back trajectories of this air parcel indicate that its origin was the Asian continent, where it was convected aloft, transported at high speeds at high altitudes, and then subsided over the eastern Pacific [*Fuelberg et al.*, 2001; *Clarke et al.*, 2001]. Estimates for high altitude, midlatitude, NO_x lifetimes of 3–9 days have been estimated by *Davis et al.* [1996] based on the fall PEM-West A data. Although clearly an interesting observation, due to the infrequency of airborne sampling at these lower altitudes at midlatitudes, insufficient data exists in the CENP region to accurately evaluate how important these events might be in regulating background levels of NO_x.

3.7. Water

[48] The springtime water vapor levels (ppmv) are shown in Figure 12a. Although not evident from the plot due to the scale selection, the latitudinal trend in BL H_2O ranges from 25,000 ppm (0°–5°N) to 5,000 ppm at 40°–45°N. A modest latitudinal trend is also evident at higher altitudes. Values in the tropical zone over the altitude range of 2–6 km are factors of 2 to 3 higher than those at midlatitudes. Clearly, the strongest gradient evident during springtime is not latitudinal but altitudinal. The mixing ratio of H_2O in the lower 2 km of the troposphere typically is more than an order of magnitude larger than that found between 5 and 9 km. Above 9 km, levels fall to below 200 ppm, and therefore lie two orders of magnitude below those in the tropical marine boundary layer.

[49] The BL fall water gradient is found to vary much less than spring ranging from 21,000 to 12,000 ppm over the latitude range of 0°–5° to 40°–45°N, respectively. Quite interestingly, above the BL only a very modest latitudinal trend in water is found. However, the altitudinal trend for fall, like that for spring, is still quite strong, encompassing an order of magnitude decrease from the surface to 5–8 km.

[50] The major seasonal difference in the water level distribution is the increase seen in midlatitude values during the fall. This reflects the fact that the seasonal temperature cycle and the coupled water cycle lag behind insolation, particularly in this marine setting [*Yienger et al.*, 1999]. As a result, spring water levels are influenced by the late winter insolation, while fall levels are influenced by the late summer insolation. An analysis of tropospheric water vapor using NASA's Water Vapor Project (NVAP) data set concluded that, for 1988–1992, northern hemisphere water vapor reached a minimum in February and peaked in August [*Randel et al.*, 1996]. The total water vapor (surface to 300 mb) increased by 88% from the minimum to maximum. The lack of any major seasonal variation in tropical insolation results in little variation in water vapor mixing ratios at these latitudes.

3.8. Nonmethane Hydrocarbons

[51] A wide range of nonmethane hydrocarbons have been sampled during the various airborne campaigns in the Pacific [*Blake et al.*, 2001, and references therein]. Two of these hydrocarbons, propane and ethyne, are presented here in Figures 12c–12f. Both species have intermediate lifetimes due to oxidation by OH, typically ranging from 1 to 4 weeks. The springtime distribution of propane, as seen in Figure 12c, shows a large latitudinal gradient. Tropical BL propane concentrations typically do not exceed 20 pptv, but increase to as much 280–350 pptv in the transitional zone, and increase yet further to 350+ pptv upon reaching the midlatitudes. This general pattern also holds true at higher altitudes; however, the onset of high values at the higher altitudes does not occur until 25°N is reached. A similar pattern can be seen for ethyne, with two differences being that ethyne has modestly higher mixing ratios and that the onset of higher mixing ratios occurs at a lower latitude (e.g., 15°N) at the higher elevations.

[52] By contrast, during fall neither propane or ethyne shows a significant latitudinal gradient. Equally important is that the maximum mixing ratios for both are substantially lower (i.e., factors of 5 to 10). Mixing ratios associated with tropical conditions during spring are found as far north as 45°N. Peak BL propane concentrations never exceed 70 pptv.

[53] While the general pattern of elevated springtime concentrations of NMHC's at the transition and midlatitude zones resembles that of CO, there tends to be a sharper latitudinal and seasonal gradient present in the case of the NMHC's. This primarily reflects the latter species' shorter lifetime. For example, rather than the 1–4 weeks cited above for propane and ethyne, CO lifetimes can range from 1 to 3 months, depending on OH levels. As will be discussed in greater detail in the companion paper by *DiNunno et al.* [2002], the relatively low levels of NMHC's across the CENP region have only a minor influence on ozone formation rates for this North Pacific region.

4. Summary

[54] Numerous airborne campaigns in the North Pacific over the last two decades have provided an opportunity to assemble an early effort at an atmospheric chemical climatology for this region. Without question, this initial effort will undergo updates in the future as more and more data become available from both aircraft and satellite platforms.

[55] In the current treatment, the ensemble data have been examined for seasonal, latitudinal, and altitudinal trends for several critical photochemical precursor species (e.g., O_3, CO, NO, H_2O). This chemical record should prove valuable as a baseline for examining future changes to this region due

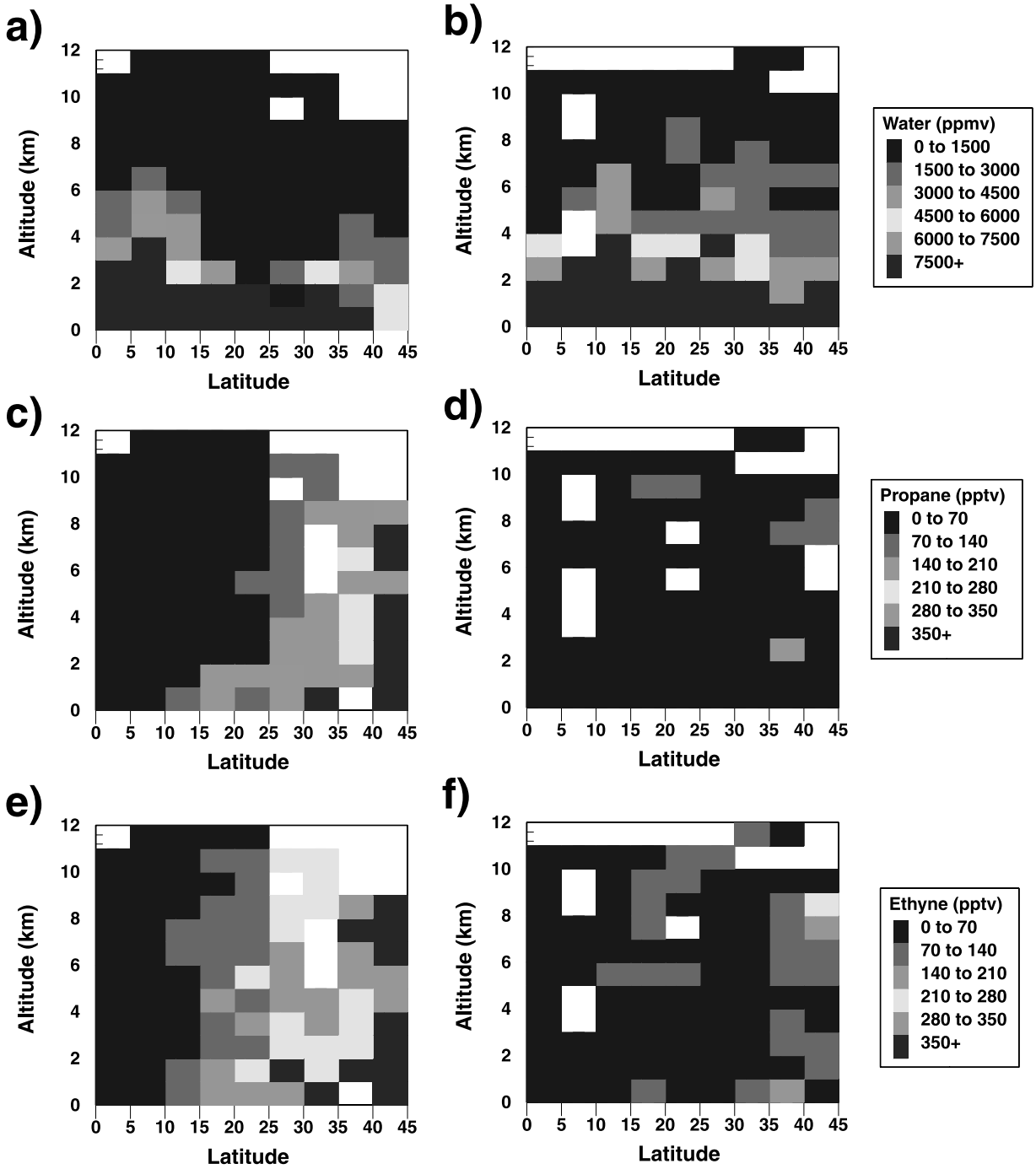

Figure 12. Seasonal altitudinal/latitudinal photochemical precursor distributions derived from airborne ensemble database. Data is segregated into 5 degree latitude and 1 km altitude bins. Values plotted are medians for: (a) water, spring; (b) water, fall; (c) C_3H_8, spring; (d) C_3H_8, fall; (e) C_2H_2, spring; (f) C_2H_2, fall. See color version of this figure at back of this issue.

to increasing Asian Pacific-Rim industrial development. The database assembled here revealed that significant seasonal shifts do occur in all precursors. Not surprisingly, the most significant of these shifts involved the transition (15°–30°N) and midlatitude (30°–45°N) zones.

[56] In the specific case of ozone, the sharpest seasonal gradient was found to occur in the transition zone, with this zone looking more like the midlatitudes in spring, but like the tropics during fall. Observed ozone values in the transition zone during spring exceeded those in fall by 20 ppbv. The overall trends in the airborne data were found to be generally in good agreement with other observational data involving other sampling strategies [*Fishman et al.*, 1990; *Oltmans and Levy*, 1994], as well as with model simulations [*Yienger et al.*, 1999]. The ensemble aircraft data, however, have added an important dimension to the overall picture in that it has provided detailed vertical profiles for ozone beyond the latitudinal range of current

ozonesonde stations within the CENP region. It has also provided detailed vertical structure for ozone over a large region where only total column ozone values were previously available.

[57] Significant CENP seasonal and latitudinal trends were also noted for CO. Surface stations in the Pacific have for many years been reporting higher CO levels at higher latitudes. The aircraft data has shown that this trend exists at all altitudes. It also has revealed that for the midlatitudes, a C-shaped altitudinal pattern with concentrations highest in the midlatitudes, appears to be present both in the spring and fall. These CO trends appear to reflect the climatological wind fields and associated long range transport. Strong seasonal patterns in CO appear to highlight the strong seasonal variations in the main CO sink, the OH radical. The midlatitude minimum in OH during winter combined with a relatively long lifetime for CO result in a spring peak. The springtime maximum of biomass burning in Central and northern South America also coincides with tropical low altitude enhancements seen in CO. On the other hand, high OH in summer leads to a CO minimum in August which continue into the fall months.

[58] The airborne NO_x data ensemble has shown that, in general, low levels dominate the entire CENP region. Modest BL latitudinal variations were found with the midlatitude and the transition zones showing factors of 2 to 3 times higher values than for the tropics. A second trend was that, for some latitudes, a significant increase in NO_x occurred with increasing altitude, with the fall season at tropical latitudes being the most important example of this. Because of the absence of natural surface sources and the continuous loss of NO_x via oxidation to HNO_3 it appears that BL NO_x is at least partially maintained through decomposition of subsiding PAN [*Moxim et al.*, 1996]. Still another source identified in the PEM-Tropics B data involves the lofting, long range transport, and subsidence of concentrated Asian emissions/plumes into the CENP region. However, the small temporal and geographic nature of these plumes makes it difficult to establish their frequency, given the intermittent nature of aircraft sampling. Thus, the overall impact from these plumes is yet to be quantified. At higher altitudes, considerable evidence was found showing that lightning plays a major role in controlling NO_x levels, with the most favorable time for local lightning events occurring in fall.

[59] Water, as expected, showed a modest tendency toward higher concentrations in the tropics, and also revealed a strong altitudinal trend. Levels were found to decrease by an order of magnitude between the surface and 5–9 km. A significant seasonal variation was also found for the midlatitude zone, with fall water mixing ratios exceeding those in spring. The mixing ratios of the NMHC's generally followed the patterns observed for CO. Given that the most likely source and sink (e.g., continental emissions and reaction with OH) are in common, this pattern is not surprising. In comparison to CO, shorter lived NMHC's like C_3H_8 tend to have sharper seasonal latitudinal gradients when comparing spring and fall.

[60] When comparisons were possible, the results from this airborne based study tended to agree with previous sampling strategies used to compile precursor databases for the CENP region. The advantages of the current data set is that it greatly expands upon the altitudinal and geographical coverage for each precursor species; thus permitting a more comprehensive examination of the ozone budget for this region as has been carried out in the companion paper by *DiNunno et al.* [2002].

[61] **Acknowledgments.** The authors would like to acknowledge the partial support of this research from NASA grant NCC-1-306. We also would like to thank the NOAA_CIRES Climate Diagnostics Center, Boulder, Colorado for the use of the NCEP reanalysis data and NASA for the use of the MAPS CO data from the NASA Langley Research Center Atmospheric Sciences Data Center. Long-term carbon monoxide data was obtained from National Oceanic and Atmospheric Administration, Climate Monitoring and Diagnostics Laboratory (CMDL), Carbon Cycle Group.

References

Atlas, E. L., and B. A. Ridley, The Mauna Loa Observatory Photochemistry Experiment: Introduction, *J. Geophys. Res.*, *101*, 14,531–14,541, 1996.

Bates, T. S., B. J. Huebert, J. L. Gras, F. B. Griffiths, and P. A. Durkee, International Global Atmospheric Chemistry (IGAC) Project's First Aerosol Characterization Experiment (ACE 1): Overview, *J. Geophys. Res.*, *103*, 16,297–16,318, 1998.

Beck, S. M., et al., Operational overview of NASA GTE/CITE 1 airborne instrument intercomparisons: Carbon monoxide, nitric oxide, and hydroxyl instrumentation, *J. Geophys. Res.*, *92*, 1977–1985, 1987.

Blake, D. R., T.-Y. Chen, T. W. Smith Jr., C. J.-L. Wang, O. W. Wingenter, N. J. Blake, F. S. Rowland, and E. W. Mayer, Three-dimensional distribution of nonmethane hydrocarbons and halocarbons over the northwestern Pacific during the 1991 Pacific Exploratory Mission (PEM-West A), *J. Geophys. Res.*, *101*, 1763–1778, 1996.

Blake, N. J., D. R. Blake, T.-Y. Chen, J. E. Collins Jr., G. W. Sachse, B. E. Anderson, and F. S. Rowland, Distributions and seasonality of selected hydrocarbons and halocarbons over the western Pacific basin during PEM-West A and PEM-West B, *J. Geophys. Res.*, *102*, 28,315–28,331, 1997.

Blake, N. J., et al., Influence of southern hemispheric biomass burning on midtropospheric distributions of nonmethane hydrocarbons and selected halocarbons over the remote South Pacific, *J. Geophys. Res.*, *104*, 16,213–16,232, 1999a.

Blake, N. J., et al., Aircraft measurements of the latitudinal, vertical, and seasonal variations of NMHCs, methyl nitrate, methyl halides, and DMS during the First Aerosol Characterization Experiment (ACE 1), *J. Geophys. Res.*, *104*, 21,803–21,818, 1999b.

Blake, N. J., et al., Large-scale latitudinal and vertical distributions of NMHC's and selected halocarbons in the troposphere over the Pacific Ocean during the March–April 999 Pacific Exploratory Mission (PEM-Tropics B), *J. Geophys. Res.*, *106*, 32,637–32,644, 2001.

Bradshaw, J., D. Davis, G. Grodzinsky, S. Smyth, R. Newell, S. Sandholm, and S. C. Liu, Observed distributions of nitrogen oxides in the remote free troposphere from the NASA global tropospheric experiment programs, *Rev. Geophys.*, *38*, 61–116, 2000.

Carroll, M. A., et al., Aircraft measurements of NO_x over the eastern Pacific and continental United States and implications for ozone production, *J. Geophys. Res.*, *95*, 10,205–10,233, 1990.

Chameides, W. L., D. Davis, M. Rodgers, J. Bradshaw, S. Sandholm, G. Sachse, G. Hill, G. Gregory, and R. Rasmussen, Net ozone photochemical production over the eastern and central north Pacific as inferred from GTE/CITE-1 observations during fall 1983, *J. Geophys. Res.*, *92*, 2131–2152, 1987.

Chameides, W. L., D. Davis, G. Gregory, G. Sachse, and A. Torres, Ozone precursors and ozone photochemistry over eastern North Pacific Ocean during the spring of 1984 based on the NASA GTE/CITE 1 airborne observations, *J. Geophys. Res.*, *94*, 9799–9808, 1989.

Chen, G., et al., An assessment of HOx chemistry in the tropical Pacific boundary layer: Comparison of model simulations with observations recorded during PEM Tropics A, *J. Atmos. Chem.*, *38*, 317–344, 2001.

Christian, H. J., R. J. Blakeslee, and S. J. Goodman, The detection of lightning from geostationary orbit, *J. Geophys. Res.*, *94*, 13,329–13,337, 1989.

Christopher, S. A., J. Chou, R. M. Welch, D. V. Kliche, and V. S. Connors, Satellite investigations of fire, smoke and carbon monoxide during April 1994 MAPS mission: Case studies over tropical Asia, *J. Geophys. Res.*, *103*, 19,237–19,336, 1998.

Clarke, A. D., W. G. Collins, P. J. Rasch, V. N. Kasputin, K. Moore, S. Howell, and H. E. Fuelberg, Dust and pollution transport on global scales: Aerosol measurements and model predictions, *J. Geophys. Res.*, *106*, 32,555–32,569, 2001.

Connors, V. S., B. B. Gormsen, S. Nolf, and H. G. Reichle Jr., Spaceborne observations of the global distribution of carbon monoxide in the middle troposphere during April and October 1994, *J. Geophys. Res.*, *104*, 21,455–21,470, 1999.

Crawford, J. H., et al., Implications of large scale shifts in tropospheric NO_x levels in the remote tropical Pacific, *J. Geophys. Res.*, *102*, 28,447–28,468, 1997a.

Crawford, J. H., et al., An assessment of ozone photochemistry in the extratropical western north Pacific: Impact of continental outflow during the late winter/earlier spring, *J. Geophys. Res.*, *102*, 28,469–28,487, 1997b.

Crawford, J. H., et al., Assessment of upper tropospheric HOx sources over the tropical Pacific based on NASA GTE/PEM data: Net effect on HOx and other photochemical parameters, *J. Geophys. Res.*, *104*, 16,255–16,273, 1999.

Davis, D. D., Project Gametag: An overview, *J. Geophys. Res.*, *85*, 7285–7292, 1980.

Davis, D. D., J. D. Bradshaw, M. O. Rodgers, S. T. Sandholm, and S. KeSheng, Free tropospheric and boundary layer measurements of NO over the central and eastern North Pacific Ocean, *J. Geophys. Res.*, *92*, 2049–2070, 1987.

Davis, D. D., et al., Assessment of the ozone photochemistry tendency in the western North Pacific as inferred from PEM-West A observations during the fall of 1991, *J. Geophys. Res.*, *101*, 2111–2134, 1996.

DiNunno, B., D. Davis, G. Chen, J. Crawford, J. Olson, and S. Liu, An assessment of ozone photochemistry in the central/eastern North Pacific as determined from multiyear airborne field studies, *J. Geophys. Res.*, doi:10.1029/2001JD001468, in press, 2002.

Emmons, L. K., D. A. Hauglustaine, J.-F. Muller, M. A. Carroll, G. P. Brassuer, D. Brunner, J. Staehlin, V. Thouret, and A. Marenco, Data composites of airborne observations of tropospheric ozone and its precursors, *J. Geophys. Res.*, *105*, 20,497–20,538, 2000.

Fishman, J., and V. G. Brackett, The climatological distribution of tropospheric ozone derived from satellite measurements using version 7 Total Ozone Mapping Spectrometer and Stratospheric Aerosol and Gas Experiment data sets, *J. Geophys. Res.*, *102*, 19,275–19,278, 1997.

Fishman, J., and P. Crutzen, The origin of ozone in the troposphere, *Nature*, *274*, 855–858, 1978.

Fishman, J., C. Watson, J. Larsen, and J. Logan, Distribution of tropospheric ozone determined from satellite data, *J. Geophys. Res.*, *95*, 3599–3617, 1990.

Fuelberg, H. E., R. E. Newell, D. J. Westberg, J. C. Maloney, J. R. Hannan, B. D. Martin, M. A. Avery, and Y. Zhu, A meteorological overview of the Second Pacific Exploratory Mission in the Tropics, *J. Geophys. Res.*, *106*, 32,427–32,443, 2001.

Goldenbaum, G. C., and R. R. Dickerson, Nitric oxide production by lightning discharges, *J. Geophys. Res.*, *98*, 18,333–18,338, 1993.

Gregory, G. L., J. M. Hoell Jr., A. L. Torres, M. A. Carroll, B. A. Ridley, M. O. Rodgers, J. Bradshaw, S. Sandholm, and D. D. Davis, An intercomparison of airborne nitric oxide measurements: A second opportunity, *J. Geophys. Res.*, *95*, 10,129–10,138, 1990.

Hao, W. M., and M.-H. Liu, Spatial and temporal distribution of tropical biomass burning in 1980 with 5 × 5 resolution, *Global Biogeochem. Cycles*, *8*, 495–503, 1994.

Heidt, L. E., J. P. Krasnec, R. A. Lueb, W. H. Pollock, B. E. Henry, and P. J. Crutzen, Latitudinal distributions of CO and CH_4 over the Pacific, *J. Geophys. Res.*, *85*, 7329–7336, 1980.

Hess, P. G., N. Srimani, and S. J. Flocke, Trajectories and related variations in the chemical composition of air for the Mauna Loa observatory during 1991 and 1992, *J. Geophys. Res.*, *101*, 14,543–14,568, 1996.

Hoell, J. M., Jr., G. L. Gregory, D. S. McDougal, M. A. Carroll, M. McFarland, B. A. Ridley, D. D. Davis, J. Bradshaw, M. O. Rodgers, and A. L. Torres, An intercomparison of nitric oxide measurement techniques, *J. Geophys. Res.*, *90*, 12,843–12,851, 1985.

Hoell, J. M., Jr., G. L. Gregory, D. S. McDougal, A. L. Torres, D. D. Davis, J. Bradshaw, M. O. Rodgers, B. A. Ridley, and M. A. Carroll, Airborne intercomparison of nitric oxide measurement techniques, *J. Geophys. Res.*, *92*, 1995–2008, 1987a.

Hoell, J. M., Jr., G. L. Gregory, D. S. McDougal, G. W. Sachse, G. F. Hill, E. P. Condon, and R. A. Rasmussen, Airborne intercomparison of carbon monoxide measurement techniques, *J. Geophys. Res.*, *92*, 2009–2019, 1987b.

Hoell, J., M., Jr., D. L. Albritton, G. L. Gregory, R. J. McNeal, S. M. Beck, R. J. Bendura, and J. W. Drewy, Operational overview of the NASA GTE/CITE 2 airborne instrument intercomparisons: Nitrogen dioxide, nitric acid, and peroxyacetyl nitrate, *J. Geophys. Res.*, *95*, 10,047–10,054, 1990.

Hoell, J., M., Jr., D. D. Davis, S. C. Liu, R. Newell, M. Shipham, H. Akimoto, R. J. McNeal, R. J. Bendura, and J. W. Drewry, Pacific Exploratory Mission-West (PEM-West A): September–October 1991, *J. Geophys. Res.*, *101*, 1641–1653, 1996.

Hoell, J. M., Jr., D. D. Davis, S. C. Liu, R. E. Newell, H. Akimoto, R. J. McNeal, and R. J. Bendura, Pacific Exploratory Mission-West (PEM-West B): February–March, 1994, *J. Geophys. Res.*, *102*, 28,223–28,239, 1997.

Hoell, J. M., Jr., D. D. Davis, D. J. Jacob, M. O. Rogers, R. E. Newell, H. E. Fuelberg, R. J. McNeal, J. L. Raper, and R. J. Bendura, Pacific Exploratory Mission in the tropical Pacific: PEM-Tropics A, August–September, 1996, *J. Geophys. Res.*, *104*, 5567–5583, 1999.

Holloway, T., H. Levy II, and P. Kasibhatla, Global distribution of carbon monoxide, *J. Geophys. Res.*, *105*, 12,123–12,147, 2000.

Horowitz, L. W., and D. J. Jacob, Global impact of fossil fuel combustion on atmospheric NOx, *J. Geophys. Res.*, *104*, 22,823–23,840, 1999.

Jacob, D. J., J. A. Logan, and P. P. Murti, Effect of rising Asian emissions on surface ozone in the United States, *Geophys. Res. Lett.*, *26*, 2175–2178, 1999.

Jaffe, D., A. Mahura, J. Kelley, J. Atkins, P. C. Novelli, and J. Merrill, Impact of Asian emissions on the remote North Pacific atmosphere: Interpretation of CO data from Shemya, Guam, Midway, and Mauna Loa, *J. Geophys. Res.*, *102*, 28,627–28,635, 1997.

Jaffe, D., et al., Transport of Asian air pollution to North America, *Geophys. Res. Lett.*, *26*, 711–714, 1999.

Khalil, M. A. K., and R. A. Rasmussen, Carbon monoxide in the Earth's atmosphere: Increasing trend, *Science*, *224*, 54–56, 1984.

Khalil, M. A. K., and R. A. Rasmussen, Carbon monoxide in the Earth's atmosphere: Indications of a global increase, *Nature*, *332*, 242–245, 1988.

Khalil, M. A. K., and R. A. Rasmussen, Global decrease in atmospheric carbon monoxide concentration, *Nature*, *370*, 639–641, 1994.

Kok, G. L., A. S. H. Prevot, R. D. Schillawski, and J. E. Johnson, Carbon monoxide measurements from 76 N to 59 S and over the South Tasman Sea, *J. Geophys. Res.*, *103*, 16,731–16,736, 1998.

Kondo, Y., H. Ziereis, M. Koike, S. Kawakami, G. L. Gregory, G. W. Sachse, H. B. Singh, D. D. Davis, and J. T. Merrill, Reactive nitrogen over the Pacific Ocean during PEM-West A, *J. Geophys. Res.*, *101*, 1809–1828, 1996.

Kondo, Y., S. Kawakami, M. Koike, D. W. Fahey, H. Nakajima, Y. Zhao, N. Toriyama, M. Kanada, G. W. Sachse, and G. L. Gregory, Performance of an aircraft instrument for the measurement of NO_y, *J. Geophys. Res.*, *102*, 28,663–28,671, 1997.

Lelieveld, J., and F. J. Dentener, What controls tropospheric ozone?, *J. Geophys. Res.*, *105*, 3531–3551, 2000.

Levy, H., II, J. D. Mahlman, W. J. Moxim, and S. C. Liu, Tropospheric ozone: The role of transport, *J. Geophys. Res.*, *90*, 3753–3771, 1985.

Levy, H., II, W. J. Moxim, and P. S. Kasibhatla, A global three-dimensional time-dependent lightning source of tropospheric NO_x, *J. Geophys. Res.*, *101*, 22,911–22,922, 1996.

Liu, S. C., D. Kley, M. McFarland, J. D. Mahlman, and H. Levy II, On the origin of tropospheric ozone, *J. Geophys. Res.*, *85*, 7546–7552, 1980.

Logan, J. A., An analysis of ozonesonde data for the troposphere: Recommendations for testing 3-D models and development of a gridded climatology for tropospheric ozone, *J. Geophys. Res.*, *104*, 16,115–16,149, 1999.

Logan, J. A., M. J. Prather, S. C. Wofsy, and M. B. McElroy, Tropospheric chemistry: A global perspective, *J. Geophys. Res.*, *86*, 7210–7254, 1981.

Marenco, A., et al., Measurement of ozone and water vapor by Airbus in-service aircraft: The MOZAIC airborne program, an overview, *J. Geophys. Res.*, *103*, 25,631–25,642, 1998.

Merrill, J. T., Trajectory results and interpretation for PEM-West A, *J. Geophys. Res.*, *101*, 1679, 1996.

Monks, P. S., A review of the observations and origins of the spring ozone maximum, *Atmos. Environ.*, *34*, 3545–3561, 2000.

Moxim, W. J., H. Levy II, and P. S. Kasibhatla, Simulated global tropospheric PAN: Its transport and impact on NOx, *J. Geophys. Res.*, *101*, 12,621–12,638, 1996.

Novelli, P. C., L. P. Steele, and P. P. Tans, Mixing ratios of carbon monoxide in the troposphere, *J. Geophys. Res.*, *97*, 20,731–20,750, 1992.

Novelli, P. C., K. A. Masarie, and P. M. Lang, Distributions and recent changes of carbon monoxide in the lower troposphere, *J. Geophys. Res.*, *103*, 19,015–19,033, 1998.

Olson, J. R., B. A. Baum, D. R. Cahoon, and J. H. Crawford, Frequency and distribution of forest, savanna, and crop fires over tropical regions during PEM-Tropics A, *J. Geophys. Res.*, *104*, 5865–5876, 1999.

Oltmans, S. J., and H. Levy II, Surface ozone measurements from a global network, *Atmos. Environ.*, *28*, 9–24, 1994.

Oltmans, S. J., D. J. Hoffmann, J. A. Lathrop, J. M. Harris, W. D. Komhyr, and D. Kuniyuki, Tropospheric ozone during Mauna Loa Observatory Photochemistry Experiment 2 compared to long-term measurements from surface and ozonesonde observations, *J. Geophys. Res.*, *101*, 14,569–14,580, 1996.

Pickering, K. E., Y. Wang, W.-K. Tao, C. Price, and J.-F. Muller, Vertical distributions of lightning NOx for use in regional and global chemical transport models, *J. Geophys. Res.*, *103*, 31,203–31,216, 1998.

Pougatchev, N. S., G. W. Sachse, H. E. Fuelberg, C. P. Rinsland, R. B. Chatfield, V. S. Connors, N. B. Jones, J. Notholt, P. C. Novelli, and H. G. Reichle Jr., Planetary Exploratory Mission-Tropics carbon monoxide measurements in historical context, *J. Geophys. Res.*, *104*, 26,195–26,207, 1999.

Pradeep Kumar, P., G. K. Manohar, and S. S. Kandalgaonkar, Global distribution of nitric oxide produced by lightning and its seasonal variation, *J. Geophys. Res.*, *100*, 11,203–11,208, 1995.

Randel, D. L., T. H. Vonder Haar, M. A. Ringerud, G. L. Stephens, T. J. Greenwald, and C. L. Combs, A new global water vapor dataset, *Bull. Am. Meteorol. Soc.*, *77*, 1233–1246, 1996.

Raper, J. L., M. M. Kleb, D. J. Jacob, D. D. Davis, R. E. Newell, H. E. Fuelberg, R. J. Bendura, J. M. Hoell, and R. J. McNeal, Pacific Exploratory Mission in the Tropical Pacific: PEM-Tropics B, March–April 1999, *J. Geophys. Res.*, *106*, 32,401–32,425, 2001.

Reichle, H. G., Jr., V. S. Connors, J. A. Holland, W. D. Hypes, H. A. Wallio, J. C. Casas, B. B. Gormsen, M. S. Saylor, and W. D. Hesketh, Middle and Upper Tropospheric Carbon Monoxide Mixing Ratios as Measured by a Satellite-Borne Remote Sensor During November 1981, *J. Geophys. Res.*, *91*, 10,865–10,887, 1986.

Reichle, H. G., Jr., V. S. Connors, J. A. Holland, R. T. Sherrill, H. A. Wallio, J. C. Casas, E. P. Condon, B. B. Gormsen, and W. Seiler, The distribution of middle tropospheric carbon monoxide during early October 1984, *J. Geophys. Res.*, *95*, 9845–9856, 1990.

Ridley, B. A., M. A. Carroll, and G. L. Gregory, Measurements of Nitric Oxide in the Boundary Layer and Free Troposphere Over the Pacific Ocean, *J. Geophys. Res.*, *92*, 2025–2048, 1987.

Routhier, F., and D. D. Davis, Free tropospheric/boundary layer airborne measurements of H_2O over the latitude range of 58 S to 70 N: Comparison with simultaneous ozone and carbon monoxide measurements, *J. Geophys. Res.*, *85*, 7293–7306, 1980.

Routhier, F., R. Dennett, D. D. Davis, A. Wartburg, P. Haagenson, and A. C. Delany, Free tropospheric and boundary-layer airborne measurements of ozone over the latitude range of 58 S to 70 N, *J. Geophys. Res.*, *85*, 7307–7321, 1980.

Russell, L. M., D. H. Lenschow, K. K. Laursen, T. S. Bates, A. R. Bandy, and D. Thornton, Bidirectional mixing in a marine PBL overlain by a second turbulent layer, *J. Geophys. Res.*, *103*, 16,411–16,432, 1998.

Sachse, G. W., G. F. Hill, L. O. Wade, and M. G. Perry, Fast-response, high precision carbon monoxide sensor using a tunable diode laser absorption technique, *J. Geophys. Res.*, *92*, 2071–2082, 1987.

Sandholm, S., S. Smyth, R. Bai, and J. Bradshaw, Recent and future improvements in two-photon laser-induced fluorescence NO measurement capabilities, *J. Geophys. Res.*, *102*, 28,651–28,661, 1997.

Sandholm, S. T., J. D. Bradshaw, K. S. Dorris, M. O. Rodgers, and D. D. Davis, An airborne compatible photofragmentation two-photon laser-induced fluorescence instrument for measuring background tropospheric levels of NO, NO_x, and NO_2, *J. Geophys. Res.*, *95*, 10,155–10,162, 1990.

Sanhueza, E., Effects of vegetation burning on the atmospheric chemistry of the Venezuelan savanna, in *Proceedings From the Chapman Conference on Global Biomass Burning: Atmospheric, Climatic, and Biospheric Implications, 19-23 March, Williamsburg, Virginia*, edited by J. Levine, pp. 122–125, MIT Press, Camdridge, Mass., 1991.

Schultz, M. G., et al., On the origin of tropospheric ozone and NO_x over the tropical South Pacific, *J. Geophys. Res.*, *104*, 5829–5843, 1999.

Talbot, R. W., et al., Chemical characteristics of continental outflow over the tropical south Atlantic ocean from Brazil and Africa, *J. Geophys. Res.*, *101*, 24,187–24,202, 1996.

Thompson, A. M., et al., Ozone observations and a model of marine boundary layer photo-chemistry during SAGA 3, *J. Geophys. Res.*, *98*, 16,955–16,968, 1993.

Wang, Y. H., D. J. Jacob, and J. A. Logan, Global simulation of tropospheric O_3-NO_x-hydrocarbon chemistry, 1, Model formulation, *J. Geophys. Res.*, *103*, 10,713–10,725, 1998.

Yienger, J. J., A. A. Klonecki, H. Levy II, W. J. Moxim, and G. R. Carmichael, An evaluation of chemistry's role in the winter-spring ozone maximum found in the northern midlatitude free troposphere, *J. Geophys. Res.*, *104*, 3655–3667, 1999.

B. Anderson, M. Avery, A. Balok, J. Barrick, G. Gregory, G. Sachse, and S. Vay, NASA Langley Research Center, Hampton, VA, USA.

D. Blake and N. Blake, Department of Chemistry, University of California, Irvine, CA, USA.

M. Carroll, Department of Atmospheric, Oceanic, and Space Sciences, University of Michigan, Ann Arbor, MI, USA.

G. Chen, D. Davis, B. DiNunno, and S. Sandholm, Department of Earth and Atmospheric Science, Georgia Institute of Technology, Atlanta, GA, USA. (bd42@prism.gatech.edu)

H. Fuelberg and B. Martin, Department of Meteorology, Florida State University, Tallahassee, FL, USA.

F. Grahek, D. Montzka, B. Ridley, and J. Walega, Atmospheric Chemistry Division, National Center for Atmospheric Research, Boulder, CO, USA.

G. Kok, Research Aviation Facility, National Center for Atmospheric Research, Boulder, CO, USA.

Y. Kondo, Research Center for Advanced Science and Technology, University of Tokyo, Japan.

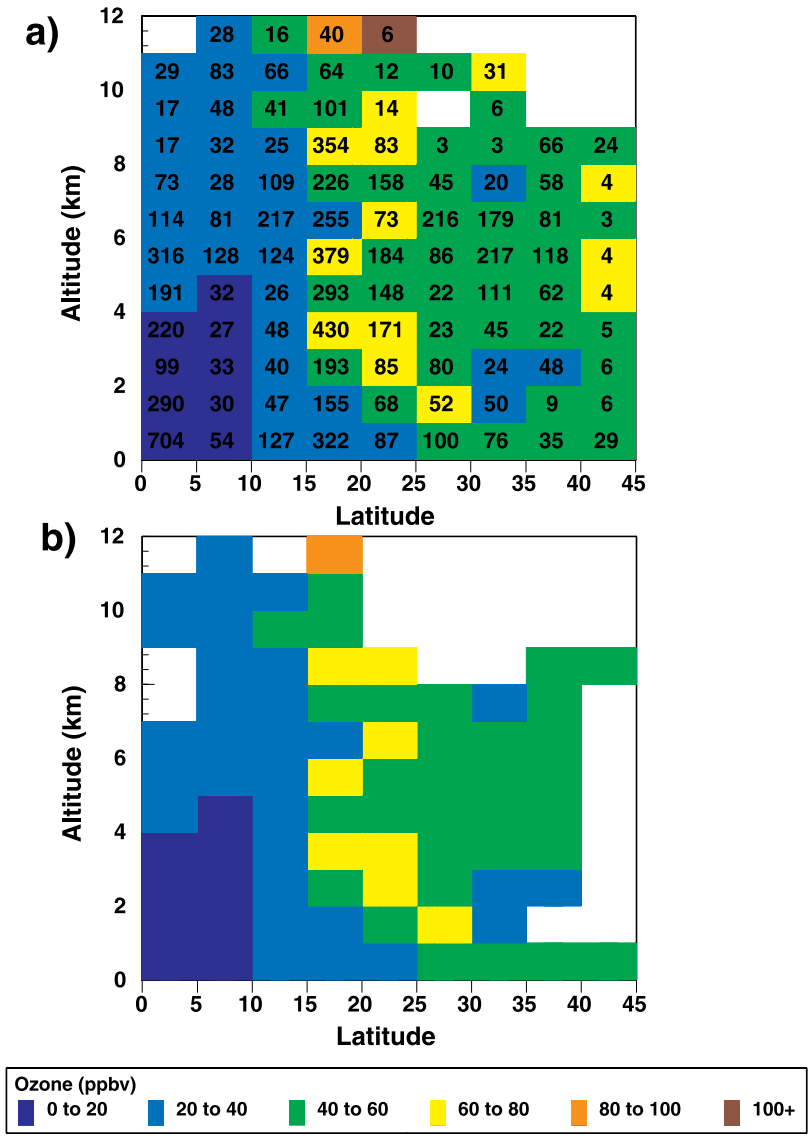

Figure 3. Low altitude, long-term seasonal climatologies for streamlines and wind speeds in the Northern Pacific basin. Profiles were generated using averaged NCEP reanalysis products from 1948 to 1999. Streamlines are in red, wind speed, and direction are represented by black arrows at 850 and 925 mb pressure levels. CENP region is enclosed in grey box. (a) spring, 850 mb; (b) fall, 850 mb; (c) spring, 925 mb; (d) fall, 925 mb.

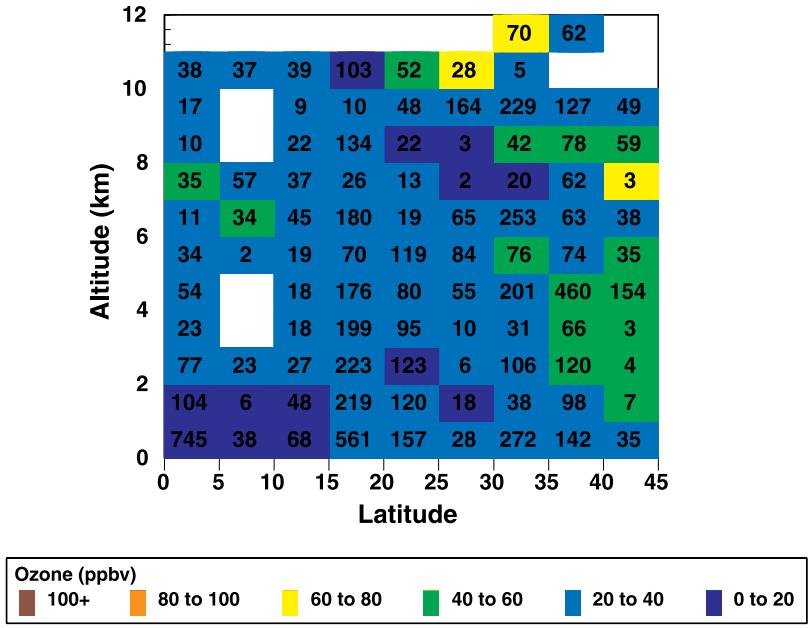

Figure 4. Seasonal lightning frequency data recorded by NASA's Optical Transient Detector. Units are number of flashes per three month season. CENP region is enclosed by outline. (a) Fall, 1996 (time period for PEM-Tropics A); (b) Spring, 1999 (time period of PEM-Tropics B).

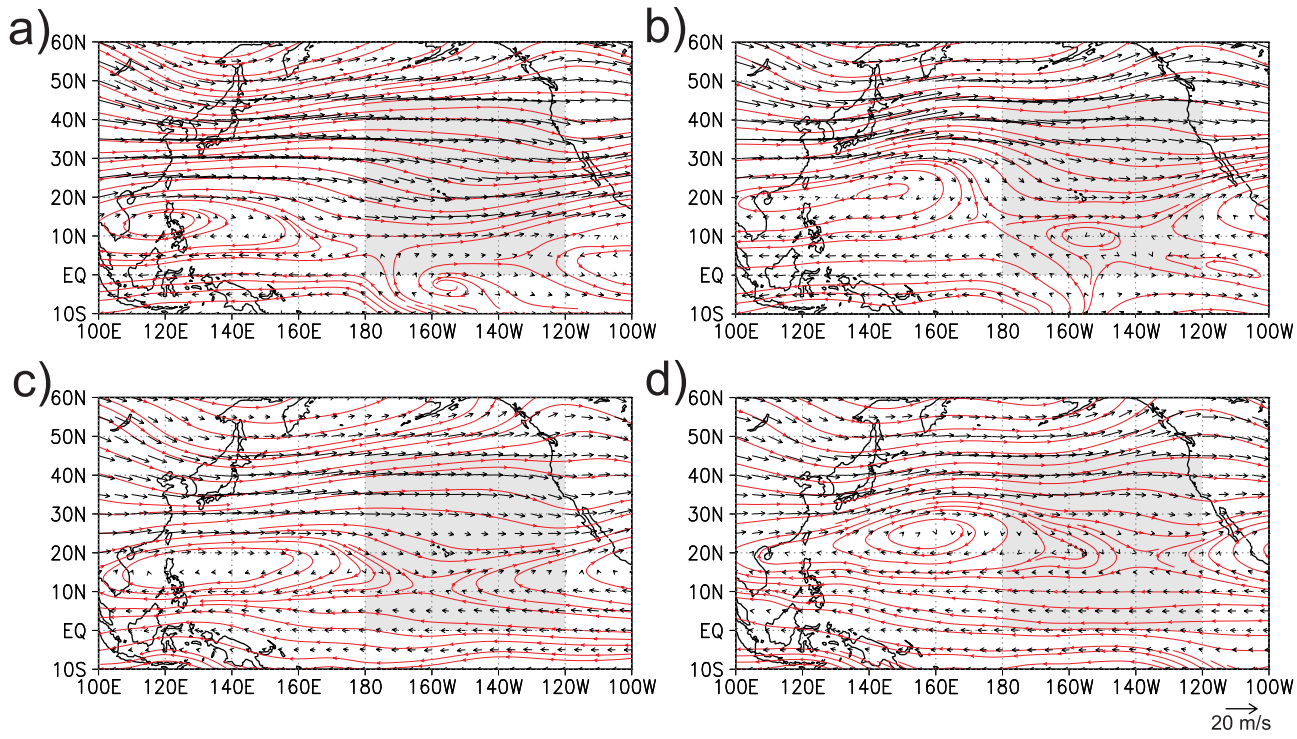

Figure 5. Seasonal altitudinal/latitudinal photochemical precursor distributions derived from airborne ensemble database. Data is segregated into 5 degree latitude and 1 km altitude bins. Values plotted are medians for: (a) O_3, spring; (b) O_3, fall; (c) CO, spring; (d) CO, fall; (e) NO_x, spring; (f) NO_x, fall. NO_x values were generated using observed NO and model generated NO_2.

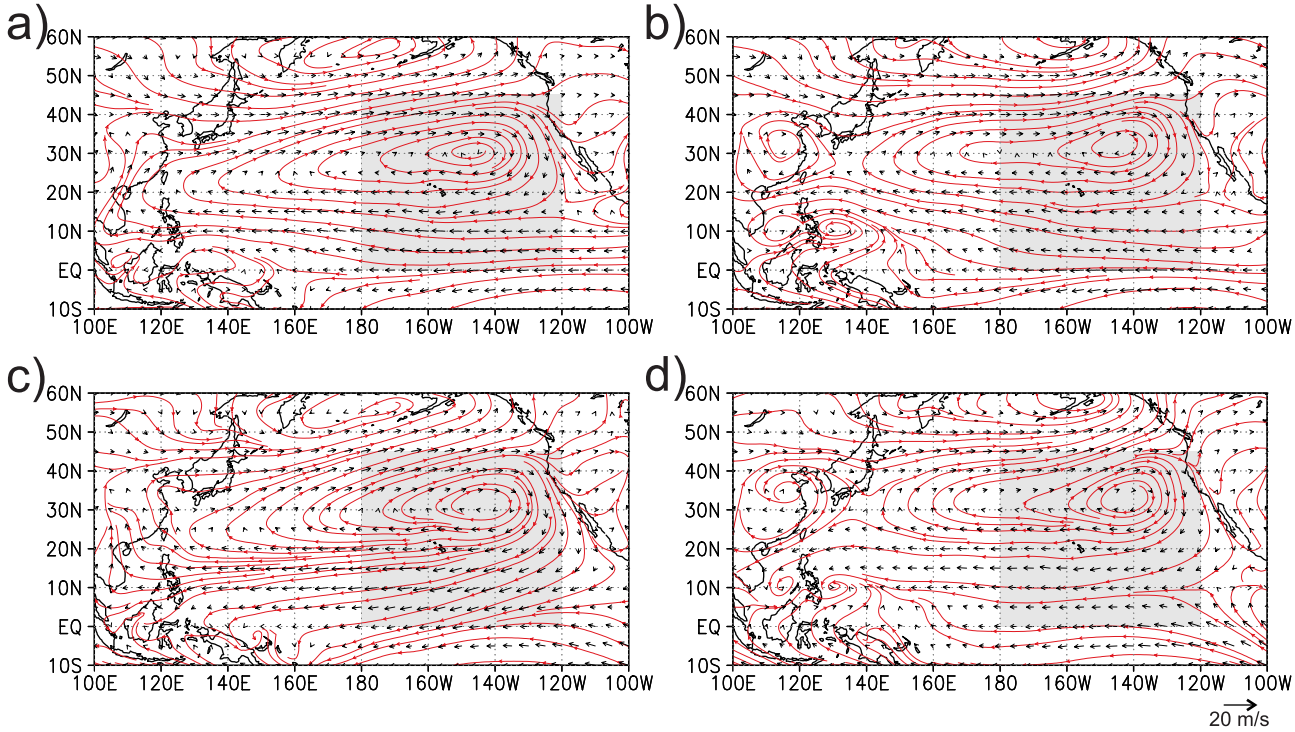

Figure 6. Comparison of ozonesonde data from Hilo, Hawaii [*Logan*, 1999] with CENP airborne O_3 database. (a) spring; (b) fall.

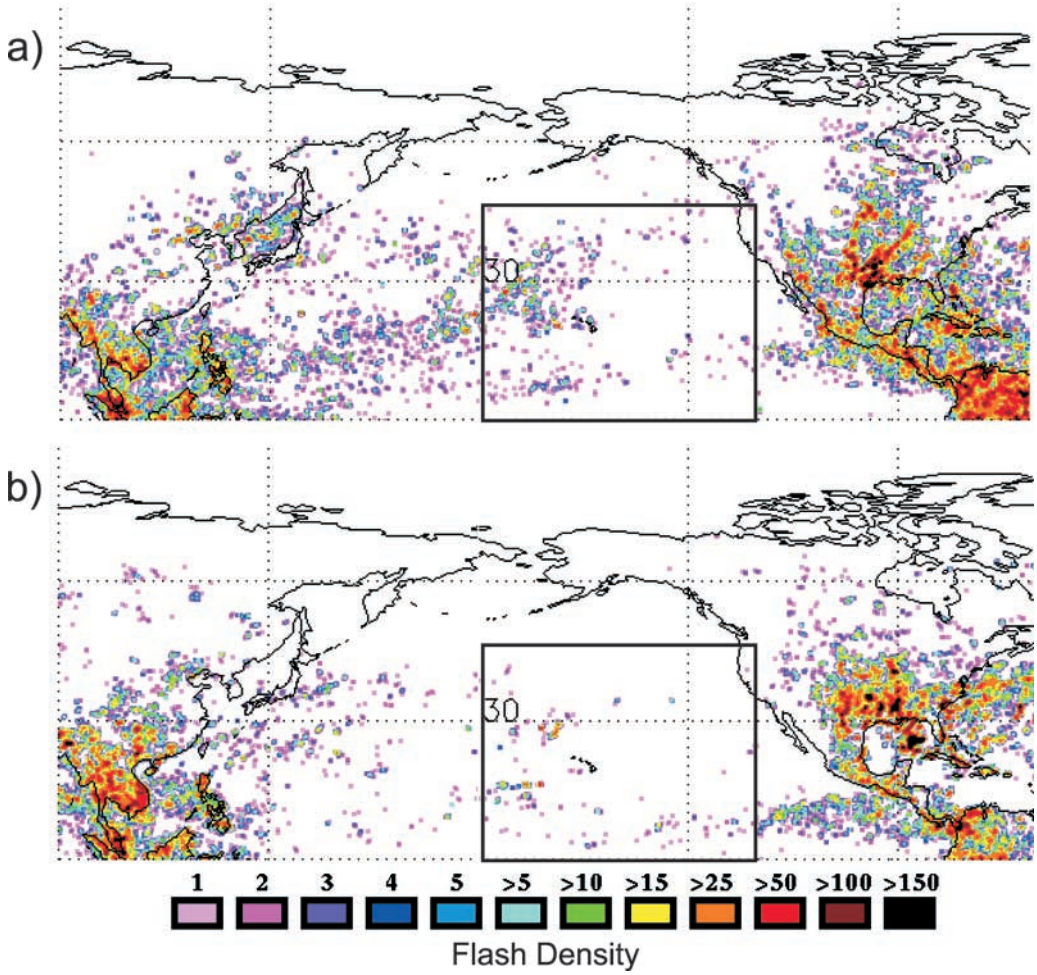

Figure 7. Long-term monthly median observations of CO recorded in the CENP region by the Climate Monitoring and Diagnostics Laboratory. a) SHM, Shemya Island, 52°N, 173°E; and MID, Midway Island, 28°N, 177°W; b) MLO, Mauna Loa, 19°N, 155°W, 3.3 km; and KUM, Cape Kumakahi, 19°N 154°W; and c) CHR, Christmas Island, 2°N 157°W. Note, all stations except for Mauna Loa are below 50 m in altitude.

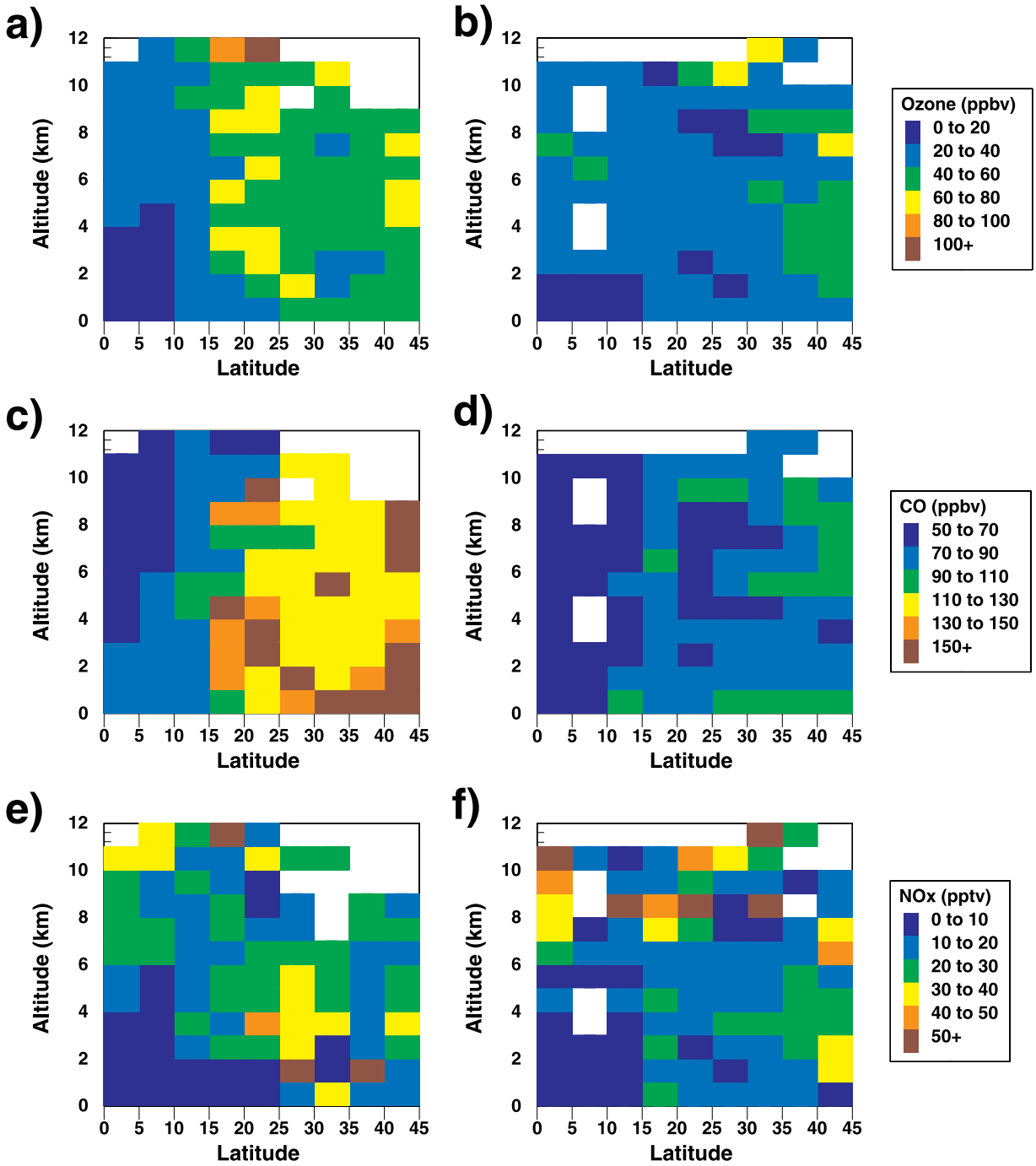

Figure 8. Multiyear airborne observations of free tropospheric CO (>2 km) as a function of distance from USA west coast. Box and whisker plot showing median, inner quartiles, and 5%/95% values for: (a) spring; (b) fall.

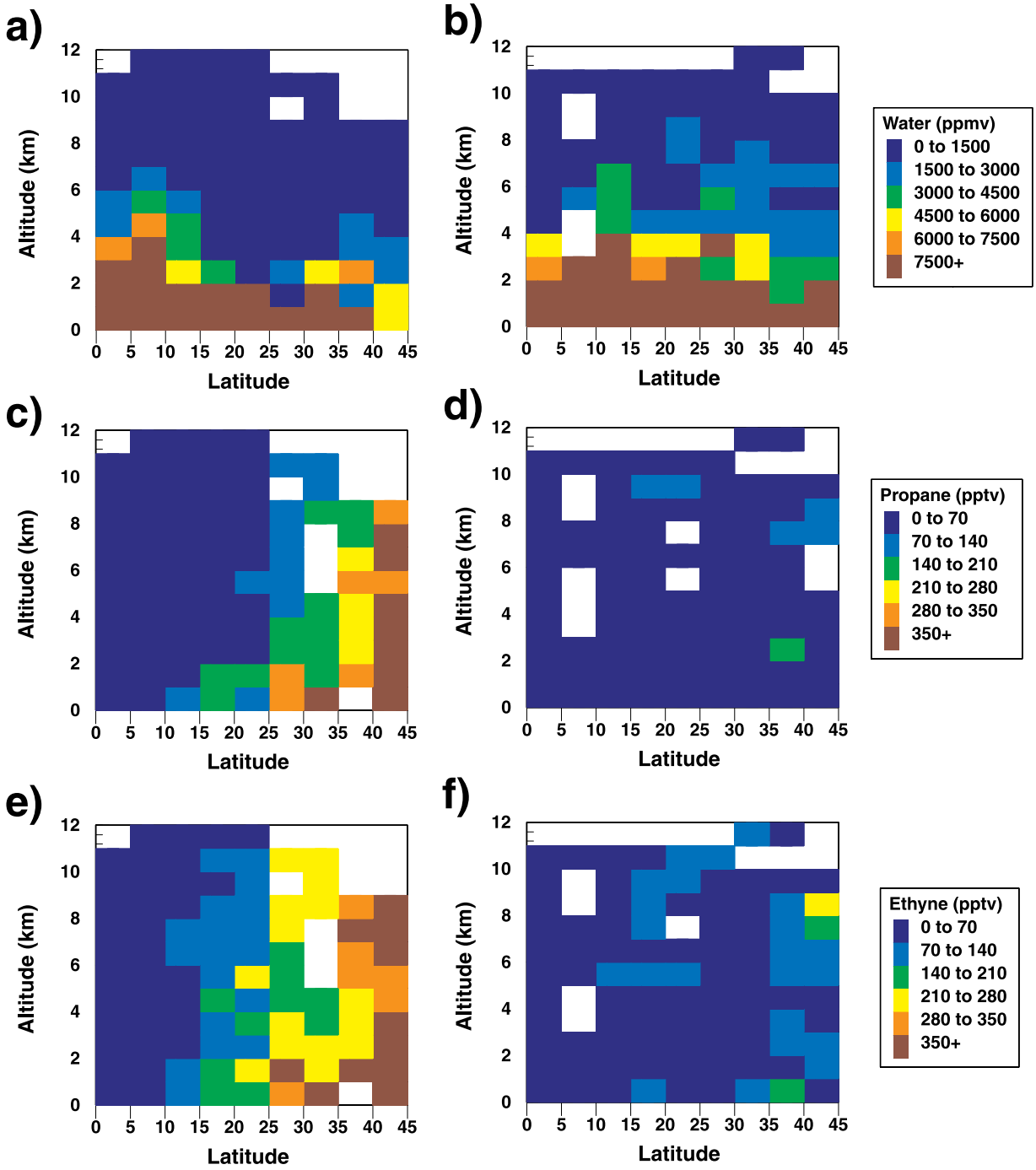

Figure 12. Seasonal altitudinal/latitudinal photochemical precursor distributions derived from airborne ensemble database. Data is segregated into 5 degree latitude and 1 km altitude bins. Values plotted are medians for: (a) water, spring; (b) water, fall; (c) C_3H_8, spring; (d) C_3H_8, fall; (e) C_2H_2, spring; (f) C_2H_2, fall.